Estimating Localized Sources of Diffusion Fields Using Spatiotemporal Sensor Measurements

John Murray-Bruce, *Student Member, IEEE*, and Pier Luigi Dragotti, *Senior Member, IEEE*

***Abstract*—We consider diffusion fields induced by a finite number of spatially localized sources and address the problem of estimating these sources using spatiotemporal samples of the field obtained with a sensor network. Within this framework, we consider two different time evolutions: the case where the sources are instantaneous, as well as, the case where the sources decay exponentially in time after activation. We first derive novel exact inversion formulas, for both source distributions, through the use of Green's second theorem and a family of sensing functions to compute generalized field samples. These generalized samples can then be inverted using variations of existing algebraic methods such as Prony's method. Next, we develop a novel and robust reconstruction method for diffusion fields by properly extending these formulas to operate on the spatiotemporal samples of the field. Finally, we present numerical results using both synthetic and real data to verify the algorithms proposed herein.**

***Index Terms*—Spatiotemporal sampling, diffusion fields, finite rate of innovation (FRI), Prony's method, sensor networks.**

I. Introduction

RECENTLY, the use of wireless sensor networks for environmental monitoring has been a topic of intensive research. The sensor nodes obtain spatiotemporal samples of physical fields over the region of interest. For most cases these fields are driven by well-known partial differential equations (PDE) with the diffusion and wave equations being typical examples. In this paper, we concentrate on processes governed by the diffusion equation. An efficient and robust sampling and reconstruction strategy for such fields will impact several real-life applications, from the detection of pollution and plume sources [3] in environmental monitoring to controlling the spread of fungal diseases in precision agriculture [4], as well as retracing the sources of biochemical and nuclear wastes and leakages [5]–[7]. Furthermore, understanding the distribution of hot and cold spots due to energy inefficiencies in processors [8], [9], as well as, large data center clusters [10] can lead to better load balancing.

Manuscript received September 23, 2014; revised February 06, 2015; accepted March 23, 2015. Date of publication April 02, 2015; date of current version May 11, 2015. The associate editor coordinating the review of this manuscript and approving it for publication was Dr. Ashish Pandharipande. This work is supported by the European Research Council (ERC) starting investigator award Nr. 277800 (RecoSamp). Some of the work in this paper has, in part, been presented in the Thirty-Ninth IEEE International Conference on Acoustics, Speech and Signal Processing (ICASSP), Florence, Italy, May 2014 [1], and the European Signal Processing Conference (EUSIPCO), Lisbon, Portugal, September 2014 [2].

The authors are with the Communications and Signal Processing Group, Department of Electrical and Electronic Engineering, Imperial College, London SW7 2AZ, U.K. (e-mail: john.murray-bruce07@imperial.ac.uk; p.dragotti@imperial.ac.uk).

Color versions of one or more of the figures in this paper are available online at http://ieeexplore.ieee.org.

Digital Object Identifier 10.1109/TSP.2015.2419187

A lot of recent research has concentrated on developing sensor data fusion schemes that aim to either, infer the sources inducing the field [11]–[16] or to reconstruct directly the field [17]–[19]. Diffusion fields are typically non-bandlimited and hence require a dense set of samples for a faithful recovery under the bandlimited (BL) framework [20]. Ranieri and Vetterli [21] suggest that in some interesting cases, specifically when the initial field distribution is not important, a BL reconstruction is sufficient since the spatial bandwidth decays exponentially fast with time and frequency. To alleviate the limitation of BL reconstruction, Reise *et al.* [18], [22] propose the use of *hybrid shift-invariant spaces*, since these spaces allow the modeling of smooth non-BL fields without imposing strict band-limitation. They investigate the use of B-splines for static fields and extend their construction to time-varying fields using an iterative procedure. In [9] Ranieri *et al.* also propose a subspace-based method for successfully recovering *thermal maps*; in this case, an optimal low-dimensional approximation is used, by first estimating the principal bases—*eigenmaps*—through an experiment carried out at design-time. Techniques based on the use of finite element method (FEM) [23], [24] to solve the static field reconstruction problem have also been researched. For example, van Waterschoot and Leus [19], [25] propose to combine the spatiotemporal samples with the PDE-based field model to achieve static field estimation at certain points of interest. Furthermore, a compressed sensing (CS) approach is proposed in [13] and is extended to incorporate the diffusion equation model in [26].

For non-static fields however, it is common to first estimate the sources of the field as this allows complete field reconstruction in space and time. Statistical estimation methods, see [27]–[30] and the references therein, based on Bayesian estimation and Kalman filtering have been proposed. In addition, Le Niliot *et al.* propose to estimate the sources using boundary element methods (BEM) [16] and validate their proposed iterative algorithm through real-life experiments [31]. In [5] Matthes *et al.* develop a single source localization algorithm based on continuous concentration measurements of the field. Dokmanic *et al.* [11] retrieve the single source parameters by approximating the single source field using a truncated Fourier series, whereas Lu *et al.* demonstrate that by solving a set of linear equations the single source parameters can be estimated [14]. In addition, Lu and Vetterli propose two methods for source estimation, namely spatial super-resolution [32] and an adaptive scheme for sources with smooth spatial distributions [33]; whilst the Finite Difference Time Domain method is used to achieve source localization and signal reconstruction of acoustic pressure fields in [34]. We note that existing schemes based on FEM may require the use of dense meshes for a faithful recovery of the field, whilst compressed sensing-based

schemes rely on uniform spatial sampling which is often difficult to achieve in practice. A more realistic assumption is a uniform placement of nodes but subjected to some random jitter [35]. Furthermore some of these existing methods make no assumptions on the temporal nature of the sources, and so are more generally applicable, but they may become unstable in the presence of noise or unable to fully reconstruct the entire field in both space and time.

In this paper, we focus on developing efficient and robust sampling and reconstruction schemes that can properly operate given arbitrary spatial samples of the diffusion field. Specifically, we consider the problem of sampling and reconstructing, diffusion fields induced by spatially localized sources and consider two cases: sources localized in space and instantaneous in time, and sources with a localized but time-varying/non-instantaneous distribution. Works in the area have predominantly focused on locating the sources of the field, we will however consider estimating all the source parameters including their initial intensities, activation times, as well as the decay coefficient for non-instantaneous sources.

The main contribution of this paper is two-fold. First, we provide a simple and exact closed-form inversion formula to the diffusion equation driven by a finite number of spatially localized sources. Specifically, we derive two inversion formulas, depending on the temporal nature of the sources inducing the field—instantaneous or non-instantaneous, respectively. Through the use of Green's second theorem, we show that the diffusion field can be combined using a family of well-chosen sensing functions to yield a sequence which can then be annihilated using Prony's method [36], [37] to reveal the desired source parameters. The second aspect of our contribution is to adapt these inversion formulas to address the problem of sampling and reconstructing diffusion fields. Specifically, given discrete spatiotemporal measurements of the field obtained with a network of arbitrarily distributed sensors, we provide robust reconstruction schemes that successfully recover the field by estimating the sources that induced it.

This paper is organized as follows. We formally present the sampling and reconstruction problem formulation in Section II. In Section III, we derive novel and exact closed-form expressions for jointly recovering multiple diffusion sources, given continuous field measurements. Then in Section IV, the inversion formulas obtained are adapted to the real setting where only discrete spatiotemporal sensor measurements of the field are available; we also propose ways to tackle noise and model mismatch. Simulation results are presented in Section V to show the performance of our algorithm on both synthetic and real data. Finally we provide some concluding remarks in Section VI.

II. Problem Formulation

We consider the problem of reconstructing two dimensional diffusion fields from its spatiotemporal samples. Specifically, we focus on the case where the spatiotemporal samples of the field are obtained by a network of randomly deployed sensors (see Fig. 1). Denote by $u(\mathbf{x},t)$ the diffusion field at location $\mathbf{x}\in\mathbb{R}^2$ and time t, induced by some unknown source distribution $f(\mathbf{x},t)$ within the two-dimensional region Ω. In such a setting the field will propagate Ω according to the diffusion equation,

$$\frac{\partial}{\partial t}u(\mathbf{x},t)=\mu\nabla^2 u(\mathbf{x},t)+f(\mathbf{x},t), \tag{1}$$

where μ is the diffusivity of the medium through which the field propagates. Moreover, from the theory of Green's functions this PDE has solution:

$$u(\mathbf{x},t)=(g*f)(\mathbf{x},t), \tag{2}$$

where

$$g(\mathbf{x},t)=\frac{1}{4\pi\mu t}e^{-\frac{\|\mathbf{x}\|^2}{4\mu t}}H(t) \tag{3}$$

is the Green's function of the two-dimensional diffusion field and $H(t)$ is the unit step function. The result in (2) implies that the entire field $u(\mathbf{x},t)$ can be perfectly reconstructed provided the source distribution $f(\mathbf{x},t)$ is known exactly. Therefore, this paper will concentrate on estimating the source distribution f given spatiotemporal samples of the field. We will focus our discussions on fields induced by M localized sources and, for clarity, we split the problem into the following two cases:

($\boldsymbol{\mathcal{P}\cdot 1}$) *Instantaneous Sources:* Sources are localized in both space and time with the following parameterization:

$$f(\mathbf{x},t)=\sum_{m=1}^{M}c_m\delta(\mathbf{x}-\boldsymbol{\xi}_m,t-\tau_m), \tag{4}$$

where $c_m,\tau_m\in\mathbb{R}$ are the intensity and activation time of the m-th source respectively and $\boldsymbol{\xi}_m\in\Omega$ is the source location, specifically $\boldsymbol{\xi}_m=(\xi_{1,m},\xi_{2,m})$. Under this assumption, the field reconstruction problem is equivalent to estimating the parameters $\{c_m,\boldsymbol{\xi}_m,\tau_m : m=1,\dots,M\}$ from the spatiotemporal samples $\varphi_n(t_l)=u(\mathbf{x}_n,t_l)$ of the field u. Here, $\mathbf{x}_n\in\Omega$ is an arbitrary spatial location corresponding to the position of sensor n with $n=1,\dots,N$ and t_l, for $l=0,1,\dots,L$ are the instants at which the sensors measure the field.

($\boldsymbol{\mathcal{P}\cdot 2}$) *Non-instantaneous Sources:* Sources are localized in space but exponentially decaying in time after activation, as follows:

$$f(\mathbf{x},t)=\sum_{m=1}^{M}c_m e^{\alpha_m(t-\tau_m)}\delta(\mathbf{x}-\boldsymbol{\xi}_m)H(t-\tau_m), \tag{5}$$

where $\alpha_m<0$ is the decay coefficient. Similarly, this assumption reduces the field reconstruction problem to estimating the parameters $\{\alpha_m,c_m,\boldsymbol{\xi}_m,\tau_m : m=1,\dots,M\}$ given spatiotemporal samples $\varphi_n(t_l)=u(\mathbf{x}_n,t_l)$ of the field u with $n=1,\dots,N$ and $l=0,\dots,L$.

III. Closed-Form Inversion Formulas

In this section, we derive exact inversion formulas for diffusion fields induced by spatially localized sources; both the instantaneous and non-instantaneous source distributions are considered. We demonstrate, in both cases, through the use of Green's second theorem that given access to generalized measurements of the form:

$$\mathcal{Q}(k,r)=\langle\Psi_k(\mathbf{x})\Gamma_r(t),f\rangle=\int_\Omega\int_t\Psi_k(\mathbf{x})\Gamma_r(t)f(\mathbf{x},t)\,\mathrm{d}t\,\mathrm{d}V,$$

it is possible to uniquely determine the unknown source parameters in $f(\mathbf{x},t)$. Here, V is the variable of integration performed over Ω (a surface in 2D), $\Psi_k(\mathbf{x})$ and $\Gamma_r(t)$ are properly chosen *sensing functions*. Specifically, we show that the generalized measurements $\mathcal{Q}(k,r)$ for $k,r\in\mathbb{Z}$ are given by a weighted-sum

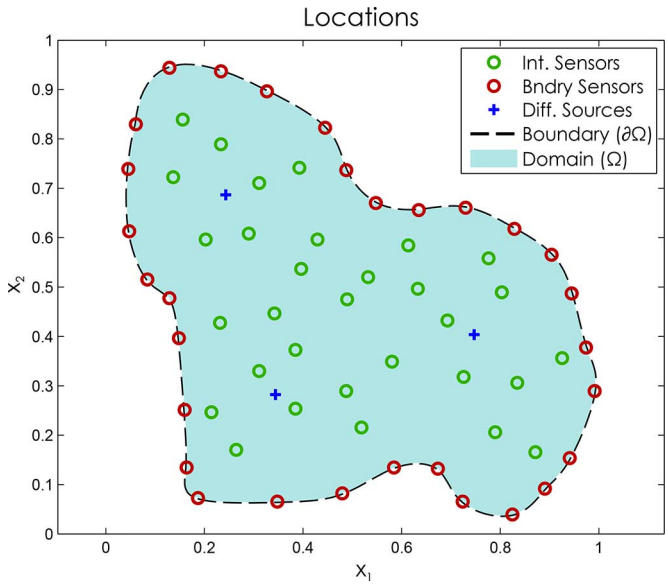

Fig. 1. An arbitrary sensor placement and the monitored domain Ω.

of complex exponentials. Moreover, given a sum of exponentials of the form $\mathcal{Q}(k,r) = \sum_{m=1}^{M} c_m e^{-k(\xi_{1,m}+\mathrm{j}\xi_{2,m})} e^{-\mathrm{j}r\tau_m/T}$, where $\mathrm{j} = \sqrt{-1}$, we then demonstrate how to map uniquely the weights and exponents of this sum to the unknown source parameters in $f(\mathbf{x},t)$ using Prony's method. This method is frequently encountered in spectral estimation [37]and in the finite rate of innovation (FRI) framework [38]–[41] and, for completeness, a brief overview is provided in Appendix A.

The use of Green's second theorem here allows us to relate, in a simple yet precise way, the boundary and interior measurements of the field, to the sources inducing the field. This is the basis of the *reciprocity gap* method [42] used in non-destructive testing of solids [42], [43]; it has also been exploited for the identification of heat sources from boundary measurements [44] and for estimating the sources of static fields governed by *Poisson's equation* in [45]. In this contribution, we propose an extension of the reciprocity gap method to the identification of instantaneous and non-instantaneous sources of diffusion in both space and time, whilst exploiting the use of more stable sensing functions.

Although the inversion formulas derived herein are based on continuous full-field measurements, which are generally inaccessible in reality, they provide insights on how to combine the discrete spatiotemporal sensor measurements in order to obtain the generalized sequence $\mathcal{Q}(k,r)$, or at least an approximation of it, which then allows for source recovery using Prony's method.

A. Diffusion Fields of Multiple Instantaneous Sources

We begin by relating the continuous diffusion field $u(\mathbf{x},t)$ in Ω to the source parameters. Let Ψ_k be a twice differentiable function in Ω, then Green's second identity relates the boundary integral and the integral over the bounded region as follows:

$$\oint_{\partial\Omega} (\Psi_k \nabla u - u\nabla\Psi_k)\cdot\hat{\mathbf{n}}_{\partial\Omega}\mathrm{d}S = \int_{\Omega}(\Psi_k\nabla^2 u - u\nabla^2\Psi_k)\mathrm{d}V, \quad (6)$$

where $\hat{\mathbf{n}}_{\partial\Omega}$ is the outward pointing unit normal vector to the boundary $\partial\Omega$ of Ω. Moreover, if Ψ_k satisfies

$$\frac{\partial\Psi_k}{\partial t} + \mu\nabla^2\Psi_k = 0 \quad (7)$$

in Ω, then given that $u(\mathbf{x},t)$ satisfies (1) we may substitute $\nabla^2\Psi_k = -\frac{1}{\mu}\frac{\partial\Psi_k}{\partial t}$ and $\nabla^2 u = \frac{1}{\mu}\left(\frac{\partial u}{\partial t} - f\right)$ into the right hand side (RHS) of (6) to obtain:

$$\begin{aligned}\oint_{\partial\Omega} (\Psi_k\nabla u - u\nabla\Psi_k)\cdot\hat{\mathbf{n}}_{\partial\Omega}\mathrm{d}S &= \frac{1}{\mu}\int_{\Omega}\Psi_k\left(\frac{\partial u}{\partial t} - f\right) + u\frac{\partial\Psi_k}{\partial t}\mathrm{d}V \\ &= \frac{1}{\mu}\int_{\Omega}\Psi_k\frac{\partial u}{\partial t} + u\frac{\partial\Psi_k}{\partial t} - \Psi_k f\,\mathrm{d}V \\ &= \frac{1}{\mu}\int_{\Omega}\frac{\partial}{\partial t}(u\Psi_k) - \Psi_k f\,\mathrm{d}V.\end{aligned}$$

Finally multiplying through by μ and rearranging yields:

$$\int_{\Omega}\frac{\partial}{\partial t}(u\Psi_k)\mathrm{d}V - \mu\oint_{\partial\Omega}(\Psi_k\nabla u - u\nabla\Psi_k)\cdot\hat{\mathbf{n}}_{\partial\Omega}\mathrm{d}S = \int_{\Omega}\Psi_k f\mathrm{d}V. \quad (8)$$

This integral equation gives a simple relationship between the source parameterization f and the induced field. We now establish how this expression can be used to recover the unknown source parameters:

Proposition 1: For the instantaneous source parameterization (4), providing $\Psi_k(\mathbf{x})$ is analytic and of the form $e^{-k(x_1+\mathrm{j}x_2)}$, $k = 0,1,\ldots,K$ with $K \geq 2M-1$ and $\Gamma_r(t) = e^{-\mathrm{j}rt/T}, r = 0,1,\ldots,R$ with $R \geq 1$, then the integral equation in (8) can be used to recover jointly the intensities, locations and activation times of the M instantaneous sources.

Proof: Recall (8) and, for conciseness, denote its left hand side (LHS) by $Q_k(t)$; hence it follows that $Q_k(t) = \int_{\Omega}\Psi_k f(\mathbf{x},t)\,\mathrm{d}V$. This identity holds true for any t, as such we can multiply both sides by some arbitrarily chosen window $\Gamma_r(t)$. Hence,

$$\Gamma_r(t)Q_k(t) = \Gamma_r(t)\int_{\Omega}\Psi_k f,\ \mathrm{d}V,\ \forall t.$$

Integrating this new expression over $t\in[0,T]$ yields:

$$\int_{t=0}^{T}\Gamma_r(t)Q_k(t)\,\mathrm{d}t = \int_{t=0}^{T}\Gamma_r(t)\int_{\Omega}\Psi_k f\,\mathrm{d}V\,\mathrm{d}t = \langle\Psi_k\Gamma_r, f\rangle.$$

Since $f(\mathbf{x},t)$ satisfies (4) we can write

$$\begin{aligned}&\int_{t=0}^{T}\Gamma_r(t)Q_k(t)\,\mathrm{d}t \\ &= \int_{t=0}^{T}\Gamma_r(t)\int_{\Omega}\Psi_k(\mathbf{x})\sum_{m=1}^{M}c_m\delta(\mathbf{x}-\boldsymbol{\xi}_m, t-\tau_m)\,\mathrm{d}V\,\mathrm{d}t \\ &= \sum_{m=1}^{M}c_m\int_{t=0}^{T}\Gamma_r(t)\delta(t-\tau_m)\,\mathrm{d}t\int_{\Omega}\Psi_k(\mathbf{x})\delta(\mathbf{x}-\boldsymbol{\xi}_m)\mathrm{d}V \\ &= \sum_{m=1}^{M}c_m\Gamma_r(\tau_m)\Psi_k(\boldsymbol{\xi}_m).\end{aligned}$$

Recall that because of (8), the LHS of the equation above is:

$$\begin{aligned}\int_{t=0}^{T}\Gamma_r(t)Q_k(t)\,\mathrm{d}t = \int_{t=0}^{T}\Gamma_r(t)\int_{\Omega}\frac{\partial}{\partial t}\left(u(\mathbf{x},t)\Psi_k\right)\mathrm{d}V\,\mathrm{d}t \\ -\mu\int_{t=0}^{T}\Gamma_r(t)\oint_{\partial\Omega}(\Psi_k\nabla u - u\nabla\Psi_k)\cdot\hat{\mathbf{n}}_{\partial\Omega}\,\mathrm{d}S\,\mathrm{d}t.\end{aligned}$$

At this point, it is useful to notice that this integral coincides exactly with the inner product $\langle\Psi_k\Gamma_r, f\rangle$. Moreover, evaluating

it yields an expression dependent only on k and r, for this reason we will denote it by $\mathcal{Q}(k,r)$. Specifically:

$$\mathcal{Q}(k,r) \stackrel{\text{def}}{=} \int_{t=0}^{T} \Gamma_r(t) \int_{\Omega} \frac{\partial}{\partial t}\left(u(\mathbf{x},t)\Psi_k\right) \mathrm{d}V\, \mathrm{d}t - \mu \int_{t=0}^{T} \Gamma_r(t) \oint_{\partial\Omega} (\Psi_k \nabla u - u \nabla \Psi_k)\cdot \hat{\mathbf{n}}_{\partial\Omega}\, \mathrm{d}S\, \mathrm{d}t, \quad (9)$$

for $k = 0, 1, \ldots, K$ and $r = 0, 1, \ldots, R$. Then it follows that,

$$\mathcal{Q}(k,r) = \langle \Psi_k \Gamma_r, f\rangle = \sum_{m=1}^{M} c_m \Gamma_r(\tau_m)\Psi_k(\boldsymbol{\xi}_m),$$

hence substituting the expressions $\Psi_k(\mathbf{x}) = e^{-k(x_1+\mathrm{j}x_2)}$ and $\Gamma_r(t) = e^{\mathrm{j}rt/T}$ into the above immediately gives the Vandermonde system:

$$\mathcal{Q}(k,r) = \sum_{m=1}^{M} c_m e^{-k(\xi_{1,m}+\mathrm{j}\xi_{2,m})} e^{-\mathrm{j}r\tau_m/T}. \quad (10)$$

Now (10) allows us to uniquely and simultaneously retrieve c_m, τ_m and $\boldsymbol{\xi}_m$ as follows:

For joint location and intensity recovery given M instantaneous sources, notice that the sequence obtained by setting $r = 0$ (or equivalently $\Gamma_r(t) = 1\, \forall r, t$) in (10) for $k \in \mathbb{Z}$ is governed by the following Vandermonde system:

$$\mathcal{R}(k) = \sum_{m=1}^{M} c_m e^{-k(\xi_{1,m}+\mathrm{j}\xi_{2,m})}, \quad k = 0, 1, \ldots, K \quad (11)$$

where

$$\mathcal{R}(k) \stackrel{\text{def}}{=} \mathcal{Q}(k,r)|_{r=0} = \int_{\Omega} (\Psi_k u)(\mathbf{x},T)\mathrm{d}V - \mu \oint_{\partial\Omega} (\Psi_k \nabla U - U\nabla\Psi_k)\cdot\hat{\mathbf{n}}_{\partial\Omega}\mathrm{d}S, \quad (12)$$

and $U(\mathbf{x}) = \int_0^T u(\mathbf{x},t)\,\mathrm{d}t$.

The sequence $\{\mathcal{R}(k)\}_{k=0}^{K}$ in (11) above is a weighted sum of a finite number of complex exponentials and so we can use Prony's method to retrieve uniquely the pairs $\{c_m, \boldsymbol{\xi}_m\}_{m=1}^{M}$ from the sequence, provided $K \geq 2M-1$ (see Appendix A). Then given the pairs $\{c_m, \boldsymbol{\xi}_m\}_{m=1}^{M}$, we apply Prony's method to the sequence $\{\mathcal{Q}(k,1)\}_{k=0}^{K}$ to obtain the pairs $\{c_m e^{-\mathrm{j}\tau_m/T}, \boldsymbol{\xi}_m\}_{m=1}^{M}$. Finally, we match the pairs of estimates by source locations to get $\{c_m, c_m e^{-\mathrm{j}\tau_m/T}, \boldsymbol{\xi}_m\}_{m=1}^{M}$ and from this it is straightforward to retrieve τ_m, since c_m and T are known. ∎

Remark 1: The choice of Ψ_k and Γ_r here is important. Firstly, Ψ_k has to satisfy (7) in order to obtain (8). This is why we pick Ψ_k to be analytic. Amongst the class of analytic functions, we choose Ψ_k to be the damped complex exponential for numerical stability. Similarly, whilst $\Gamma_r(t)$ can be any arbitrary function of time, again for stability reasons, we choose exponential function with purely imaginary exponent.

B. Diffusion Fields of Multiple Non-Instantaneous Sources

In what follows, we consider the field induced by non-instantaneous sources and following an approach similar to Proposition 1, we derive closed-form expressions for simultaneous recovery of the source parameters.

1) Exact Recovery of Source Locations: In Section III-A we showed that the field in Ω can be recovered when the source parameterization f is assumed to be a sum of M localized and instantaneous sources. In this section, we are instead concerned with localized and non-instantaneous sources. Indeed under this source model we show that the Prony system is preserved. As such, the localization step (discussed in Section III-A) can still reveal the locations, along with corresponding coefficients that we will refer to as the *generalized energies* of the non-instantaneous sources.

Proposition 2: For non-instantaneous source fields, with source parameterization (5), providing $\Psi_k(\mathbf{x})$ is analytic, and is chosen such that $\Psi_k(\mathbf{x}) = e^{-k(x_1+\mathrm{j}x_2)}$, then the integral equation in (8) is governed by the following Vandermonde system:

$$\mathcal{R}(k) = \sum_{m=1}^{M} c'_m e^{-k(\xi_{1,m}+\mathrm{j}\xi_{2,m})}, \quad k = 0, 1, \ldots, K \quad (13)$$

where $\mathcal{R}(k)$ is used to denote the family of definite integrals (12) for $k \in \mathbb{Z}$, and $c'_m = \frac{c_m}{\alpha_m}\left(e^{\alpha_m(T-\tau_m)} - 1\right)$ is the generalized energy of the m-th source.

Proof: Firstly substitute $\Psi_k = e^{-k(x_1+\mathrm{j}x_2)}$ into (8) and integrate both sides of the resulting equation over $t \in [0,T]$, to obtain:

$$\int_{\Omega} (\Psi_k u)(\mathbf{x},T)\mathrm{d}V - \mu \oint_{\partial\Omega} (\Psi_k \nabla U - U\nabla\Psi_k)\cdot\hat{\mathbf{n}}_{\partial\Omega}\mathrm{d}S = \int_0^T \int_{\Omega} \Psi_k f\, \mathrm{d}V\mathrm{d}t, \quad (14)$$

where as before we denote $U(\mathbf{x}) = \int_0^T u(\mathbf{x},t)\mathrm{d}t$. Notice that the left hand side of (14) coincides with (12), we will henceforth denote it by $\mathcal{R}(k)$ for brevity. However, given the non-instantaneous source parameterization for f, the power-sum series for $\mathcal{R}(k)$ is different to that obtained for instantaneous sources, but can be easily obtained by substituting (5) into the right hand side of (14) as follows:

$$\begin{aligned}
\mathcal{R}(k) &= \int_{t=0}^{T}\int_{\Omega} \Psi_k(\mathbf{x}) f(\mathbf{x},t)\mathrm{d}V\mathrm{d}t \\
&= \int_{\tau_m}^{T}\int_{\Omega} \Psi_k(\mathbf{x}) \sum_{m=1}^{M} c_m e^{\alpha_m(t-\tau_m)}\delta(\mathbf{x}-\boldsymbol{\xi}_m)\,\mathrm{d}V\mathrm{d}t \\
&= \sum_{m=1}^{M} c_m \int_{\Omega} \Psi_k(\mathbf{x})\delta(\mathbf{x}-\boldsymbol{\xi}_m)\,\mathrm{d}V \int_{\tau_m}^{T} e^{\alpha_m(t-\tau_m)}\mathrm{d}t \\
&= \sum_{m=1}^{M} c_m \Psi_k(\boldsymbol{\xi}_m)\left[\frac{1}{\alpha_m} e^{\alpha_m(t-\tau_m)}\right]_{\tau_m}^{T} \\
&= \sum_{m=1}^{M} \frac{c_m}{\alpha_m}\left(e^{\alpha_m(T-\tau_m)} - 1\right)\Psi_k(\boldsymbol{\xi}_m) \\
&= \sum_{m=1}^{M} c'_m e^{-k(\xi_{1,m}+\mathrm{j}\xi_{2,m})}
\end{aligned}$$

where $c'_m = \frac{c_m}{\alpha_m}(e^{\alpha_m(T-\tau_m)} - 1)$. ∎

Again the sequence $\{\mathcal{R}(k)\}_{k=0}^{K}$, governed by the weighted sum of exponentials (13) can be solved to recover the M lo-

cations of the instantaneous sources, as well as the generalized energies c'_m.

In the rest of this section, we establish a novel scheme for directly recovering the remaining source parameters: α_m, τ_m and c_m from the generalized energy c'_m.

Remark 2: It is easy to show, from (8), that given any arbitrary temporal parameterization of M sources, it is possible to recover their locations by evaluating the integral expression (12), for $k = 0, 1, \ldots, K$ and applying Prony's method on the resulting sequence $\{\mathcal{R}(k)\}_{k=0}^{K}$, as long as all M sources are localized in space. Specifically, one can show that $\mathcal{R}(k)$ will always take the form $\mathcal{R}(k) = \sum_{m=1}^{M} C_m e^{-k(\xi_{1,m}+\mathrm{j}\xi_{2,m})}$, $k = 0, 1, \ldots, K$, where C_m is the generalized energy given by $C_m = \int_0^T h_m(t)\mathrm{d}t$ for the generic source with parameterization $f(\mathbf{x}, t) = \sum_m h_m(t)\delta(\mathbf{x} - \boldsymbol{\xi}_m)$.

2) Exact Recovery of Decay Coefficients, Activation Times and Source Intensities: We begin by noting that $c'_m = \frac{c_m}{\alpha_m}(e^{\alpha_m(T-\tau_m)} - 1)$ for $m = 1, \ldots, M$ depends on the interval $[0, T]$ over which the time-integration, in (14), is performed; thus we may write,

$$c'_m(T) = \frac{c_m}{\alpha_m}\left(e^{\alpha_m(T-\tau_m)} - 1\right) \tag{15}$$

to emphasize this dependence.

Now assume we obtain the coefficients $\{c'_m(T) : m = 1, \ldots, M\}$ for the intervals $T = T_1, T_2 = T_1 + \Delta T$, and $T_3 = T_1 + 2\Delta T$. Then:

$$\begin{aligned} c'_m(T_1) &= \frac{c_m}{\alpha_m}\left(e^{\alpha_m(T_1-\tau_m)} - 1\right), && (16)\\ c'_m(T_2) &= \frac{c_m}{\alpha_m}\left(e^{\alpha_m(T_1+\Delta T-\tau_m)} - 1\right)\\ &= \frac{c_m}{\alpha_m}\left(e^{\alpha_m(T_1-\tau_m)}e^{\alpha_m\Delta T} - 1\right), && (17)\\ c'_m(T_3) &= \frac{c_m}{\alpha_m}\left(e^{\alpha_m(T_2+\Delta T-\tau_m)} - 1\right)\\ &= \frac{c_m}{\alpha_m}\left(e^{\alpha_m(T_2-\tau_m)}e^{\alpha_m\Delta T} - 1\right). && (18) \end{aligned}$$

Subtracting (16) from (17) and similarly (17) from (18), we obtain:

$$\begin{aligned} c'_m(T_2) - c'_m(T_1) &= \frac{c_m}{\alpha_m}\left(e^{\alpha_m(T_1-\tau_m)}e^{\alpha_m\Delta T} - e^{\alpha_m(T_1-\tau_m)}\right)\\ &= \frac{c_m}{\alpha_m}e^{\alpha_m(T_1-\tau_m)}\left(e^{\alpha_m\Delta T} - 1\right)\\ &= \frac{2c_m}{\alpha_m}e^{\alpha_m\frac{\Delta T}{2}}e^{\alpha_m(T_1-\tau_m)}\sinh(\alpha_m\Delta T/2), \end{aligned} \tag{19}$$

and,

$$c'_m(T_3) - c'_m(T_2) = \frac{2c_m}{\alpha_m}e^{\alpha_m\frac{\Delta T}{2}}e^{\alpha_m(T_2-\tau_m)}\sinh(\alpha_m\Delta T/2), \tag{20}$$

respectively. Dividing (19) by (20) yields,

$$\frac{c'_m(T_2) - c'_m(T_1)}{c'_m(T_3) - c'_m(T_2)} = \frac{e^{\alpha_m(T_1-\tau_m)}}{e^{\alpha_m(T_2-\tau_m)}} = e^{\alpha_m(T_1-T_2)}. \tag{21}$$

Therefore,

$$\alpha_m = \frac{1}{T_1 - T_2}\ln\left(\frac{c'_m(T_2) - c'_m(T_1)}{c'_m(T_3) - c'_m(T_2)}\right). \tag{22}$$

Given α_m it is then possible to retrieve the activation time of the m-th source as follows:

Divide (16) by (17),

$$\frac{c'_m(T_1)}{c'_m(T_2)} = \frac{\frac{c_m}{\alpha_m}\left(e^{\alpha_m(T_1-\tau_m)} - 1\right)}{\frac{c_m}{\alpha_m}\left(e^{\alpha_m(T_2-\tau_m)} - 1\right)} \tag{23}$$

and re-arrange to obtain,

$$\begin{aligned} e^{-\alpha_m\tau_m}\left(c'_m(T_1)e^{\alpha_m T_2} - c'_m(T_2)e^{\alpha_m T_1}\right)\\ = c'_m(T_1) - c'_m(T_2). \end{aligned}$$

This yields

$$\tau_m = \frac{1}{\alpha_m}\ln\left(\frac{c'_m(T_1)e^{\alpha_m T_2} - c'_m(T_2)e^{\alpha_m T_1}}{c'_m(T_1) - c'_m(T_2)}\right). \tag{24}$$

Finally, with access to estimates of α_m and τ_m, it is straightforward to estimate c_m using any of (16), (17), and (18). In particular

$$c_m = \frac{\alpha_m c'_m(T_i)}{e^{\alpha_m(T_i-\tau_m)} - 1}, \quad i = 1, 2, 3 \tag{25}$$

as required.

Remark 3: An interesting point to notice about the proposed framework is that, for sources lying outside the region Ω their contribution to the integral expressions (9), (12) and (14) is zero. We can leverage on this fact to still recover the sources of diffusion fields in bounded regions, i.e., when the medium through which the field propagates is finite. Specifically, the method of image sources allows us to model reflections in bounded regions as: an unbounded medium containing several virtual sources. However, the sensors enclose only the real sources, hence the real sources will be recovered because the contributions of the virtual sources to the integrals will be zero. Consequently, the inversion formulas remain valid and we are still able to estimate the unknown source parameters as far as the impermeable (or semi-permeable) boundaries of the medium are outside Ω. We will demonstrate through simulations, using both synthetic and real data, that we are able to fully recover the unknown source distribution f in the case where the field propagates a finite region with impermeable boundaries.

IV. Robust Source Estimation From Spatiotemporal Field Samples

With the insights gained and inversion formulas derived in Section III, we now consider the inversion problem given realistic spatiotemporal sensor measurements. In this new setting, we have two issues: *a)* we do not have access to continuous-field measurements and must approximate them using the sensor readings, and *b)* the measurements may be noisy, therefore the inversion formulas derived need to be adjusted to promote stability and robustness.

In Section IV-A, we address the issue of approximating the integrals in (9), (12) and (14), whilst Section IV-B tackles the issue of noisy sensor measurements. Finally,

Section IV-C presents the proposed, simultaneous and sequential, multiple source estimation algorithms.

A. Approximating Integrals From Spatiotemporal Samples

In this new setting, we do not have the luxury of continuous field measurements. Therefore given only spatiotemporal samples of the field, it is necessary to approximate the integrals in the (9), (12) and (14) using standard quadrature methods [46]. For the temporal integrals, a straightforward application of *Trapezium rule* yields a good approximation. We therefore focus only on (12) and (14), since (9) can be approximated easily from these two. For the spatial integrals, we are specifically concerned with approximating: *a)* path integrals along a boundary $(\partial\Omega)$ of Ω, as well as, *b)* surface integrals on the bounded region Ω. As usual approximating these integrals with sums relies on obtaining non-overlapping subdivisions of the domain over which the integral is performed. We denote these elements as, line segments δl_i with $i = 1, \ldots, I$, and polygonal segments Δ_j with $j = 1, \ldots, J$ that make up the path $(\partial\Omega)$ and surface (Ω) integrals respectively. Hence, for path integrals providing $\delta l_i \bigcap \delta l_j = \emptyset$ for $i \neq j$ and that $\bigcup_{i=1}^{I} \delta l_i = \partial\Omega$ then a well-known approximation exists, namely the path integral of some function $h(\mathbf{x})$ along $\partial\Omega$ is approximated as follows:

$$\oint_{\partial\Omega} h(\mathbf{x}) \mathrm{d}S \approx \sum_{i=1}^{I} \frac{[h(l_{i,1}) + h(l_{i,2})]}{2} \cdot |\delta l_i|, \qquad (26)$$

where $l_{i,1}$ and $l_{i,2}$ denote the end points of the line segment δl_i and $|\delta l_i|$ is its length.

Moreover, with surface integrals, if these non-overlapping subdivisions $\{\Delta_j\}_{j=1}^{J}$ are triangular such that $\bigcup_{i=1}^{I} \Delta_i = \Omega$ and $\Delta_i \bigcap \Delta_j = \emptyset$ for $i \neq j$, the surface integral of $h(\mathbf{x})$ over a bounded region Ω is approximated by the sum [47]:

$$\int_{\Omega} h(\mathbf{x}) \mathrm{d}V \approx \sum_{j=1}^{J} \frac{1}{3} \sum_{j'=1}^{3} h(\mathbf{v}_{j,j'}) \mathrm{Area}(\Delta_j), \qquad (27)$$

where $\{\mathbf{v}_{j,j'} : j' = 1, 2, 3\}$ are the vertices of Δ_j.

In our setup, these vertices coincide with the sensor locations, hence the triangular subdivisions depend directly on them. Denote the collection of all sensor locations by $\mathcal{S} = \{\mathbf{x}_1, \mathbf{x}_2, \ldots, \mathbf{x}_N\}$, we intend to construct non-overlapping triangular subdivisions given the set $\mathcal{S}$. This allows us to define the domains Ω and $\partial\Omega$ (its boundary) over which the surface and line integrals will be performed, respectively. In order to obtain stable approximations of these integrals, we will seek a triangulation that minimizes the occurrence of skinny triangles which can lead to numerical instabilities. The so called *Delaunay triangulation* $(\mathcal{DT})$ [48] meets this requirement. Thus given $\mathcal{S}$, its Delaunay triangulation is denoted by $\mathcal{DT}(\mathcal{S}) = \{\Delta_j\}_{j=1}^{J}$ and the union of all these subdivisions gives the *Convex Hull* $(\mathcal{CH})$ of $\mathcal{S}$, i.e., $\mathcal{CH}(\mathcal{S})$. Therefore, for a given sensor distribution, we define the bounded region Ω to be $\mathcal{CH}(\mathcal{S})$ and the convex hull boundary to be $\partial\Omega$ as shown in Fig. 2. Given this construction, we can then retrieve an approximation of the family of integrals in (12), and (14), as follows:

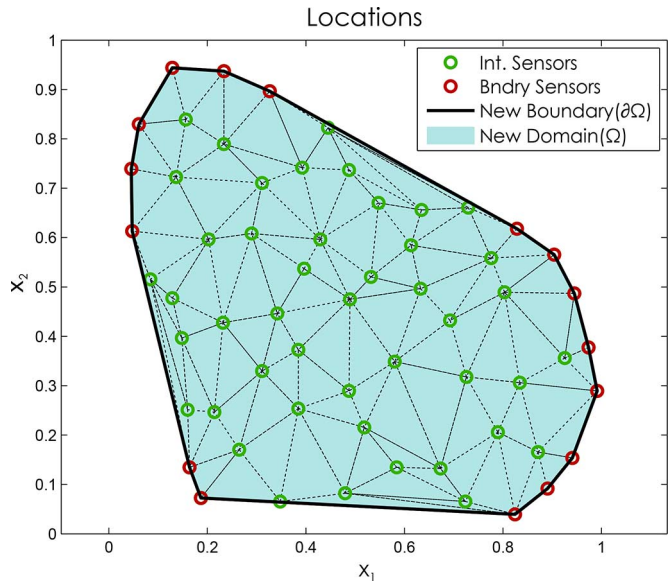

Fig. 2. An arbitrary sensor placement—the (approximate) monitored domain Ω divided into triangular meshes and the domain boundary divided into straight line segments (black solid lines).

Again let $\{\mathbf{v}_{j,j'} : j' = 1, 2, 3\}$ be the vertices of the triangular element Δ_j. Then surface integrals in (12) and (14) are approximated as follows:

$$\int_{\Omega} (\Psi_k u)(\mathbf{x}, T) \, \mathrm{d}V \approx \frac{1}{3} \sum_{j=1}^{J} \sum_{j'=1}^{3} \Psi_k(\mathbf{v}_{j,j'}) \varphi_{j,j'}(t_L) \times \mathrm{Area}(\Delta_j), \qquad (28)$$

where $\varphi_{j,j'}(t_L) = u(\mathbf{v}_{j,j'}, t_L)$ is the measurement of the sensor situated at the vertex $\mathbf{v}_{j,j'}$ at time $t = t_L$. Similarly to approximate the line integral,

$$\oint_{\partial\Omega} (\Psi_k \nabla U - U \nabla \Psi_k) \cdot \hat{\mathbf{n}}_{\partial\Omega} \, \mathrm{d}S,$$

the time integral is first approximated using trapezoidal rule, such that:

$$\begin{aligned} U(\mathbf{x}_n) &= \int_0^T u(\mathbf{x}_n, t) \mathrm{d}t \\ &\approx \left[\frac{1}{2} \left(\varphi_n(t_0) + \varphi_n(t_L) \right) + \sum_{l=1}^{L-1} \varphi_n(t_l) \right] \Delta t \end{aligned}$$

then $\nabla U(\mathbf{x}_n) = \left[\frac{\partial}{\partial x_1} U(\mathbf{x}_n), \frac{\partial}{\partial x_2} U(\mathbf{x}_n) \right]^{\top}$ is approximated using a first order central finite difference scheme, such that $\nabla U(\mathbf{x}_n) \approx [U_{x_1}(\mathbf{x}_n), U_{x_2}(\mathbf{x}_n)]^{\top}$, where $U_{x_1}(\mathbf{x}_n) \approx \frac{\partial}{\partial x_1} U(\mathbf{x}_n)$ and $U_{x_2}(\mathbf{x}_n) \approx \frac{\partial}{\partial x_2} U(\mathbf{x}_n)$ are used to denote the approximation of the field's spatial derivatives. Moreover given our choice of Ψ_k, $\nabla \Psi_k(\mathbf{x}_n) = -k \Psi_k(\mathbf{x}_n) [1, \mathrm{j}]^{\top}$. Hence,

$$\Psi_k \nabla U - U \nabla \Psi_k \approx \Psi_k(\mathbf{x}_n) \begin{bmatrix} U_{x_1}(\mathbf{x}_n) + k U(\mathbf{x}_n) \\ U_{x_2}(\mathbf{x}_n) + \mathrm{j} k U(\mathbf{x}_n) \end{bmatrix}. \qquad (29)$$

Finally for $\hat{\mathbf{n}}_{\partial\Omega} \, \mathrm{d}S$, assuming $\mathbf{x}_1, \ldots, \mathbf{x}_n, \ldots, \mathbf{x}_I \in \partial\Omega$ is a cyclically ordered set, arranged in a counterclockwise order, then:

$$\hat{\mathbf{n}}_{\partial\Omega} \approx \frac{1}{\|\mathbf{x}_n - \mathbf{x}_{n-1}\|} \begin{pmatrix} x_{2,n} - x_{2,n-1} \\ x_{1,n-1} - x_{1,n} \end{pmatrix}$$

and

$$\mathrm{d}S \approx \|\mathbf{x}_n - \mathbf{x}_{n-1}\|.$$

Therefore,

$$\oint_{\partial\Omega} (\Psi_k \nabla U - U \nabla \Psi_k) \cdot \hat{\mathbf{n}}_{\partial\Omega} \, \mathrm{d}S \approx \sum_{n=1}^{I} \Psi_k(\mathbf{x}_n) \left[(U_{x_1}(\mathbf{x}_n) + kU(\mathbf{x}_n)) (x_{2,n} - x_{2,n-1}) + (U_{x_2}(\mathbf{x}_n) + \mathrm{j}kU(\mathbf{x}_n)) (x_{1,n-1} - x_{1,n}) \right]. \quad (30)$$

Note that due to the cyclic ordering, $\mathbf{x}_0 = \mathbf{x}_I$.

B. Tackling Noise and Model Mismatch: A Subspace Denoising Approach

Given access to $K \geq 2M-1$ consecutive terms of the sequence $\{\mathcal{R}(k)\}_{k=0}^{K}$, we apply Cadzow algorithm [49] to denoise it. The basic idea of the method is as follows: when applying Prony's method on the sequence, we build a Toeplitz matrix $\mathbf{C} \in \mathbb{R}^{L_r \times L_c}$ of the form

$$\mathbf{C} = \begin{pmatrix} \mathcal{R}(L_c-1) & \mathcal{R}(L_c-2) & \cdots & \mathcal{R}(0) \\ \mathcal{R}(L_c) & \mathcal{R}(L_c-1) & \cdots & \mathcal{R}(1) \\ \vdots & \vdots & \ddots & \vdots \\ \mathcal{R}(K) & \mathcal{R}(K-1) & \cdots & \mathcal{R}(L_r-1) \end{pmatrix}, \quad (31)$$

where $M < L_r \leq L_c < K$. Moreover as highlighted in Appendix A, in the absence of noise, the rank of $\mathbf{C}$ is exactly M.

However, noisy sensor measurements and the approximation of integrals using finite sums lead to model mismatches which results in making $\mathbf{C}$ full rank. Cadzow's algorithm denoises $\mathbf{C}$ by first setting to zero the $L_r - M$ smallest singular values of $\mathbf{C}$ which are typically due to noise so as to obtain a rank M matrix, before enforcing the Toeplitz structure by averaging along the diagonals of the reconstructed low-rank matrix. The method is iterated a few times. The end result of applying Cadzow to $\mathbf{C}$ is, therefore, to denoise $\{\mathcal{R}(k)\}_{k=0}^{K}$. A similar approach is applied to $\{\mathcal{Q}(k,r)\}$.

1) Non-Instantaneous Source & Decay Coefficient Estimation With Cadzow: Consider the problem ($\boldsymbol{\mathcal{P}}\cdot\mathbf{2}$) and assume that the spatiotemporal samples are now corrupted by noise. We will examine how to improve the estimates of the unknown non-instantaneous source parameters in the presence of noise. The generation of (16), (17) and (18) using equally spaced subintervals ΔT suggests deeper underlying connections with Prony's method and its variations.

Define,

$$D_p \stackrel{\text{def}}{=} c'_m(T_{p+1}) - c'_m(T_p) = \frac{2c_m}{\alpha_m} e^{\alpha_m \frac{\Delta T}{2}} e^{\alpha_m (T_p - \tau_m)} \sinh(\alpha_m \Delta T/2). \quad (32)$$

for positive integer values of $p = 1, 2, \ldots, P$. Then it immediately follows that:

$$\mathcal{A}(p,q) \stackrel{\text{def}}{=} \frac{D_p}{D_{p+q}} = \frac{c'_m(T_{p+1}) - c'_m(T_p)}{c'_m(T_{p+q+1}) - c'_m(T_{p+q})} = \frac{\frac{2c_m}{\alpha_m} e^{\alpha_m \frac{\Delta T}{2}} e^{\alpha_m (T_p - \tau_m)} \sinh(\alpha_m \Delta T/2)}{\frac{2c_m}{\alpha_m} e^{\alpha_m \frac{\Delta T}{2}} e^{\alpha_m (T_{p+q} - \tau_m)} \sinh(\alpha_m \Delta T/2)} = \frac{e^{\alpha_m (T_p - \tau_m)}}{e^{\alpha_m (T_{p+q} - \tau_m)}} = e^{q \Delta T \alpha_m}, \quad (33)$$

where $q = 0, 1, \ldots, P-2$.

We stress that the terms $\mathcal{A}(p,q)\ \forall p,q$ are given by $\mathcal{A}(p,q) = \frac{c'_m(T_{p+1}) - c'_m(T_p)}{c'_m(T_{p+q+1}) - c'_m(T_{p+q})}$ where the c'_m's are computed by applying Prony's method to (13). Moreover, notice that for any fixed q the terms $\mathcal{A}(p,q), p = 1, 2, \ldots, P-q-1$ are equal. This is true only in the ideal scenario when there exists no model mismatches in the system, but is false in the presence of noise and other model imperfections. Assuming that the perturbations can be modelled as an approximately i.i.d process, then taking the average should give a better estimate. As such we can form a new sequence as follows:

$$\mathcal{B}(q) = \frac{1}{P-q-1} \sum_{p=1}^{P-q-1} \mathcal{A}(p,q). \quad (34)$$

It is easy to see that $\mathcal{B}(q)$ still satisfies $\mathcal{B}(q) = e^{q \Delta T \alpha_m}$, where $q = 0, 1, \ldots, P-2$. This is again a sequence where we can apply Prony's method, but with a single unknown, hence it admits a solution when $P \geq 3$. Moreover, if $P > 3$ we can also apply Cadzow's denoising algorithm to it.

The complete algorithm is summarized in Algorithm 1.

Algorithm 1: Simultaneous Estimation of M sources

Require: $\{\varphi_n(t_l)\}_{n,l}$, sensor locations $\{\mathbf{x}_n\}_n$, sampling interval Δt, SourceType.

1: Retrieve the *convex hull* ($\mathcal{CH}$) of the set of points $\{\mathbf{x}_n\}$. $\mathcal{CH}$ and its boundary define Ω and $\partial\Omega$ respectively, in (9) and (14).
2: **if** SourceType == '*instantaneous*' **then**
3: Initialize $K \geq 2M-1$ and $R \geq 1$.
4: Set window length $T = b\Delta t$ (where $b \in \mathbb{Z}, b \gg 1$).
5: Estimate sequence $\{\mathcal{Q}(k,r)\}$ for $k = 0, \ldots, K$ and $r = 0, \ldots, R$over $t \in [0, T]$ as explained in Section IV-A.
6: Denoise $\{\mathcal{Q}(k,r)\}$ using Cadzow's algorithm.
7: Apply Prony's method to $\{\mathcal{Q}(k,r)\}$ to jointly recover the unknown parameters of the M sources, i.e., $\{c_m, \boldsymbol{\xi}_m, \tau_m\}_{m=1}^{M}$.
8: **else**
9: Initialize window lengths as follows: set $T_1 = b\Delta t$ and $\Delta T = b'\Delta t$ (where $b, b' \in \mathbb{Z}, b \gg 1$ and $b' \geq 1$). Then $T_{p+1} = T_1 + p\Delta T$ for $p = 1, \ldots, P-1$.
10: Initialize $K \geq 2M-1$ and $P \geq 3$.
11: Estimate the sequence $\{\mathcal{R}(k) : k = 0, \ldots, K\}$ for each window $t \in [0, T_p]$ $p = 1, \ldots, P$, to obtain P different sequences.
12: Denoise them all using Cadzow's algorithm.
13: Apply Prony's method to each of the P sequences $\{\mathcal{R}(k)\}_{k=0}^{K}$ to find M generalized energy-location pair $\{c'_m(T_p), \boldsymbol{\xi}_m\}$ for each of the P sequences.
14: Match the P generalized energies by their corresponding locations to get: $\{c'_m(T_1), \ldots, c'_m(T_P), \boldsymbol{\xi}_m\}_{m=1}^{M}$.
15: **for** $m = 1, \ldots, M$ **do**
16: Construct $\{\mathcal{B}(q)\}$ from $\{c'_m(T_p)\}_{p=1}^{P}$ using (34).
17: Denoise $\{\mathcal{B}(q)\}$ using Cadzow.
18: For α_m apply Prony's to the denoised sequence.
19: Find τ_m and c_m using (24) and (25) respectively.
20: **end for**
21: **end if**
22: **return** $\{c_m\}_{m=1}^{M}, \{\alpha_m\}_{m=1}^{M}, \{\boldsymbol{\xi}_m\}_{m=1}^{M}$ and $\{\tau_m\}_{m=1}^{M}$.

Algorithm 2: Sequential Estimation of M Sources

Require: $\{\varphi_n(t_l)\}_{n,l}$, sensor locations $\{\mathbf{x}_n\}_n$, sampling interval Δt, SourceType.

Retrieve $\mathcal{CH}(\{\mathbf{x}_n\}_n)$.
Let $m \leftarrow 0$ and the number of valid sources $M_{vs} \leftarrow 0$.
while $m < M$ **do**
  Construct $\{\mathcal{R}(k)\}$ with $K \geq 2M' - 1$ and $M' \geq 2$.
  Estimate the M' generalized energy-location pairs $\{\sigma'_{m'}, \boldsymbol{\xi}'_{m'}\}_{m'=1}^{M'}$.
  Set M_{vs} to be the number of pairs of $\{\sigma'_{m'}, \boldsymbol{\xi}'_{m'}\}$ having both $\sigma'_{m'}$ greater than some predefined threshold and $\boldsymbol{\xi}'_{m'} \in \mathcal{CH}$.
  if $M_{vs} > 1$ **then**
    Decrease window size T and Go to 4.
  else if $M_{vs} < 1$ **then**
    Increase window size T and Go to 4.
  else if $M_{vs} == 1$ **then**
    Estimate source parameters $c_m, \boldsymbol{\xi}_m, \hat{\alpha}, \hat{\tau}$ using Algorithm 1.
    Select the $\beta \in \mathbb{N}$ nearest sensors to $\boldsymbol{\xi}_m$. For each of the β sensors, retrieve $\hat{\tau}_1^*, \ldots, \hat{\tau}_\beta^*$, and for time-varying sources $\hat{\alpha}_1^*, \ldots, \hat{\alpha}_\beta^*$ too, as described in Sections IV-C1 and IV-C2 respectively.
    $\tau_m \leftarrow \text{Ave}\{\hat{\tau}_1^*, \ldots, \hat{\tau}_\beta^*\}$, $\alpha_m \leftarrow \text{Ave}\{\hat{\alpha}_1^*, \ldots, \hat{\alpha}_\beta^*\}$.
    Reconstruct its field and adjust $\{\varphi_n(t_l)\}_{n,l}$.
    $m \leftarrow m + 1$.
    Increase window size T and Go to 4.
  end if
end while
return $\{c_m\}_{m=1}^M, \{\alpha_m\}_{m=1}^M, \{\boldsymbol{\xi}_m\}_{m=1}^M$ and $\{\tau_m\}_{m=1}^M$.

C. Sequential Estimation of Multiple Sources

Algorithm 1 can be readily used to jointly estimate multiple sources of diffusion fields from arbitrary field samples. This approach works both in the case of simultaneously activated sources or in the case of sequential activation. In the latter, however, it is more effective to estimate one source per time and to remove its contribution from the sensor measurements before estimating the next source. This is possible when: *a)* the sources have suitably distinct activation times; and *b)* the sampling interval is small enough to resolve the activation of two consecutive sources. In such a scenario, we propose the following approach. Firstly, we find a time window over which only a single source is active. We do this by examining the rank of the Toeplitz matrix constructed from $\{\mathcal{R}(k)\}$. We then estimate the source parameters as described in Algorithm 1 (with $M = 1$). Given these preliminary estimates, a selection of sensors nearest to the estimated source location are used to obtain a more precise estimate for the activation time, and when appropriate, decay coefficient of the source. These sharper estimates are obtained by performing a simple local search around the initial estimates, as follows:

1) Instantaneous Sources: Given the initial estimate of the intensity, location and activation time, $\hat{c}, \hat{\boldsymbol{\xi}}$ and $\hat{\tau}$, respectively, consider the measurements $\{\varphi_{n,l} : l = 0, \ldots, L\}$ collected by the n-th sensor (located at $\mathbf{x}_n$) and the re-synthesized sequence $\hat{\varphi}^*_{n,l} = \hat{u}(\mathbf{x}_n, t_l) = \frac{\hat{c}}{4\pi\mu(t_l - \hat{\tau}^*)} e^{-\frac{\|\mathbf{x}_n - \hat{\boldsymbol{\xi}}\|^2}{4\mu(t_l - \hat{\tau}^*)}} H(t - \hat{\tau}^*)$. By comparing the normalized inner-product between the reconstructed sequence and the measurements, we choose the $\hat{\tau}^* \in [\epsilon\hat{\tau}, \frac{1}{\epsilon}\hat{\tau}]$ where $\epsilon \in (0, 1]$ that maximizes this normalized inner product—a modification of the Cauchy-Schwarz inequality for vectors.

2) Non-Instantaneous Sources: Again we assume a single source field and the initial estimates $\hat{c}, \hat{\alpha}, \hat{\boldsymbol{\xi}}$ and $\hat{\tau}$ for the source parameters. The measured field $\{\varphi_{n,l}\}$ is compared with the reconstructed field $\{\hat{\varphi}^*_{n,l}\}$ to obtain better estimates of α and τ. In this case however, we perform a local 2D search over $\hat{\tau}^* \in [\epsilon_\tau\hat{\tau}, \frac{1}{\epsilon_\tau}\hat{\tau}]$ and $\hat{\alpha}^* \in [\epsilon_\alpha\hat{\alpha}, \frac{1}{\epsilon_\alpha}\hat{\alpha}]$ where $\epsilon_\tau, \epsilon_\alpha \in (0, 1]$ are some constants.

We perform the same search using the $\beta \in \mathbb{N}$ sensors closest to the estimated source location and obtain a final estimate for the activation time and decay coefficient, by averaging the estimates of the β sensors. The complete sequential method is summarized in Algorithm 2.

Remark 4: The strategy of selecting the β closest sensors to the estimated field is implicitly noise reducing, as these sensors will, in general, have a higher SNR since the field intensity is greater at these locations (close to the source) whilst all sensors experience the same noise power.

V. Numerical Simulations and Results

A. Simulations With Synthetic Data

The 2D diffusion field is simulated numerically in MATLAB using (2) for both source distributions (4) & (5).[1] Furthermore, spatiotemporal samples of the field are obtained by sensors randomly deployed over a square region. For noisy simulations, the spatiotemporal measurements are directly corrupted with zero mean additive white Gaussian noise (AWGN), $w_{n,l}$, as follows: $\varphi_n^{\text{noisy}}(t_l) = \varphi_n(t_l) + w_{n,l}$, so that the noise power σ_w^2 is the same for all sensors. Hence the SNR of the spatiotemporal samples is defined as:

$$\text{SNR} \stackrel{\text{def}}{=} 10\log_{10}\left(\frac{\sum_{n=1}^N \sum_{l=0}^L |\varphi_n(t_l)|^2}{N(L+1)\sigma_w^2}\right). \quad (35)$$

The numerical results presented in this section utilizes both a new arbitrary placement of sensors, as well as, a new realization of additive white Gaussian noise for each new trial.

1) Instantaneous Sources: Fig. 3 shows the parameter estimation results for sequential source estimation algorithm. The algorithm is able to recover the source parameters with high accuracy even in the noisy setting. We show results separately for 45 (top) and 63 (bottom) arbitrarily placed sensors respectively. Furthermore we present in Table I a summary of the variation of the (normalized) mean absolute error (MAE)[2] for the activation time and intensity estimates with noise, in the single source setting. The MAE decreases with increasing SNR, as expected;

[1]Consider an instantaneous source field for example, substituting (3) & (4) into (2) gives the closed form expression for the field, $u(\mathbf{x}, t) = \sum_{m=1}^M \frac{c_m}{4\pi\mu(t - \tau_m)} e^{-\frac{\|\mathbf{x} - \boldsymbol{\xi}_m\|^2}{4\mu(t-\tau_m)}} H(t - \tau_m)$. This expression can therefore be evaluated explicitly at the sensor locations $\{\mathbf{x}_n\}_n$ and sampling instants $\{t_l\}_l$ to obtain the desired spatiotemporal sensor measurements without resorting to a grid.

[2]For I total independent estimates $\hat{x}_i$ of some parameter x, the normalized mean absolute error (MAE) of x is defined here as: $\text{MAE}(x) = \frac{1}{x} \cdot \frac{\sum_{i=1}^I |x - \hat{x}_i|}{I}$.

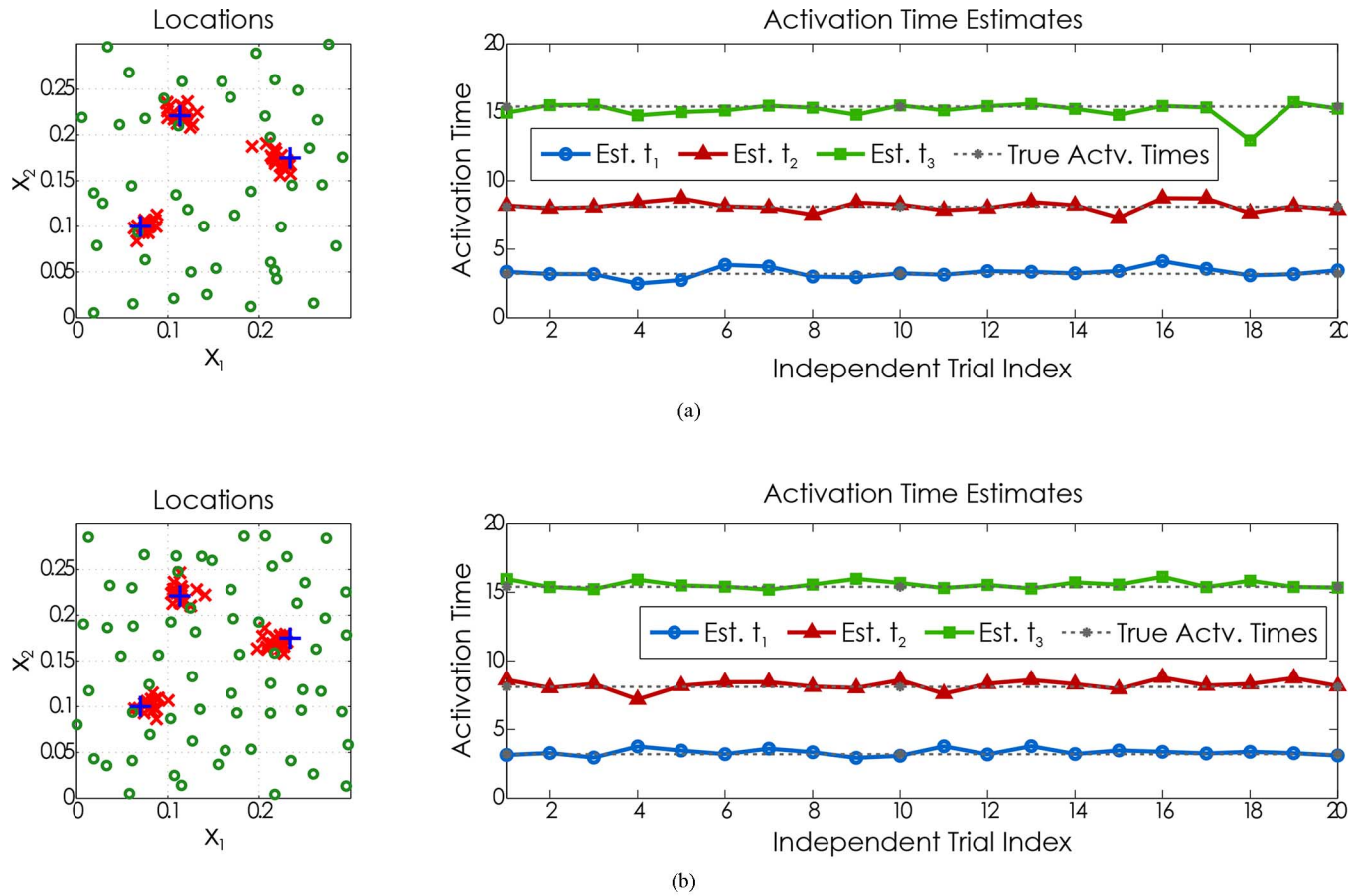

Fig. 3. Estimation of $M = 3$ diffusion sources using randomly distributed sensors. The spatiotemporal samples have SNR equal to 20 dB and the results of 20 independent trials are shown. Intensities $c_1 = c_2 = c_3 = 1$; locations $\boldsymbol{\xi}_1 = (0.113, 0.221), \boldsymbol{\xi}_2 = (0.234, 0.175), \boldsymbol{\xi}_3 = (0.070, 0.100)$; and activation times $t_1 = 3.2$ s, $t_2 = 8.1$ s, $t_3 = 15.4$ s. Field is sampled for $T_{\text{end}} = 20$ s at a frequency $\frac{1}{\Delta t} = 2$ Hz and $K = 5$ i.e., $k = 0, 1, \ldots, 5$ for the test function family $\Psi_k(\mathbf{x}) = e^{-k(x_1 + \mathrm{j}x_2)}$. The scatter-plot shows the true source locations (blue '+'), the estimated locations (red '×') and one realization of the sensor distribution (green '○'). (a) 45 Randomly distributed sensors. (b) 63 Randomly distributed sensors.

TABLE I
NORMALIZED MEAN ABSOLUTE ERROR OF SINGLE SOURCE PARAMETER ESTIMATES (500 INDEPENDENT TRIALS). FIELD IS INDUCED BY THE SINGLE INSTANTANEOUS SOURCE, $c = 1, \tau = 1.213$ S AND $\boldsymbol{\xi} = (0.1130, 0.2210)$, SAMPLED AT $f = \frac{1}{0.5} = 2$ HZ, INDEPENDENTLY WITH 45 AND 63 ARBITRARILY PLACED SENSORS, FOR $T_{\text{end}} = 8$ S. $K = 10$ FOR THE TEST FUNCTION FAMILY $\{\Psi_k\}_{k=0}^{K}$

		SNR (dB)				
		5	10	20	30	40
τ_m	45 Sensors	0.6351	0.3112	0.1653	0.1345	0.1319
	63 Sensors	0.5138	0.2267	0.0922	0.0707	0.0725
c_m	45 Sensors	0.2163	0.1500	0.1202	0.1071	0.1071
	63 Sensors	0.1610	0.1140	0.0766	0.0707	0.0698

moreover at SNR $= 10$ dB we achieve activation time resolution MAE that is much less than the sampling interval, for both sensor densities. When decreasing the SNR further, we notice the threshold effect characteristic of Prony's method in that a large jump in the MAE of the estimates is observed.

2) Non-Instantaneous Sources: Fig. 4 shows our algorithm (Algorithm 2) operating on the spatiotemporal samples of the single non-instantaneous source field. We compare the estimated parameters against their true values and the plots demonstrate that our algorithm can successfully recover the desired source parameters with good accuracy. Furthermore, we summarize the normalized MAE of the estimation algorithm in Table II.

3) Approximation Errors due to the Discretization of Integrals: In this section, we provide simulation results to demonstrate that the error due to approximating the integrals in (12) (and equivalently in (14)) does not affect the estimation of the sources of the field, in that, even at fairly high SNRs, the noise in the sensor measurements dominates the errors in the reconstruction. To this end, we compare the localization results obtained by applying Prony's method on two sequences, namely: $\{\mathcal{R}_{\text{meas}}(k)\}$ and $\{\mathcal{R}_n(k)\}$ for $k = 0, 1, \ldots, K$. $\{\mathcal{R}_{\text{meas}}(k)\}$ is constructed from noisy sensor measurements and represents the real discretized case, where (12) (and (14)) are approximated by weighted sums of the field. Conversely, $\{\mathcal{R}_n(k)\}$ is obtained by adding an equivalent noise process to the exact power-sum series, and thus represents the full-field measurement scenario, where the integrals in (12) are known precisely. Fig. 5 shows the standard deviation of the estimated spatial locations of $M = 2$ sources using $\{\mathcal{R}_{\text{meas}}(k)\}$ (dashed lines) and $\{\mathcal{R}_n(k)\}$ (solid lines) respectively. Observe that for realistic SNRs of interest, i.e., 30 dB or less, the performance of the location recovery coincides with that of the ideal, full-field measurement, case.

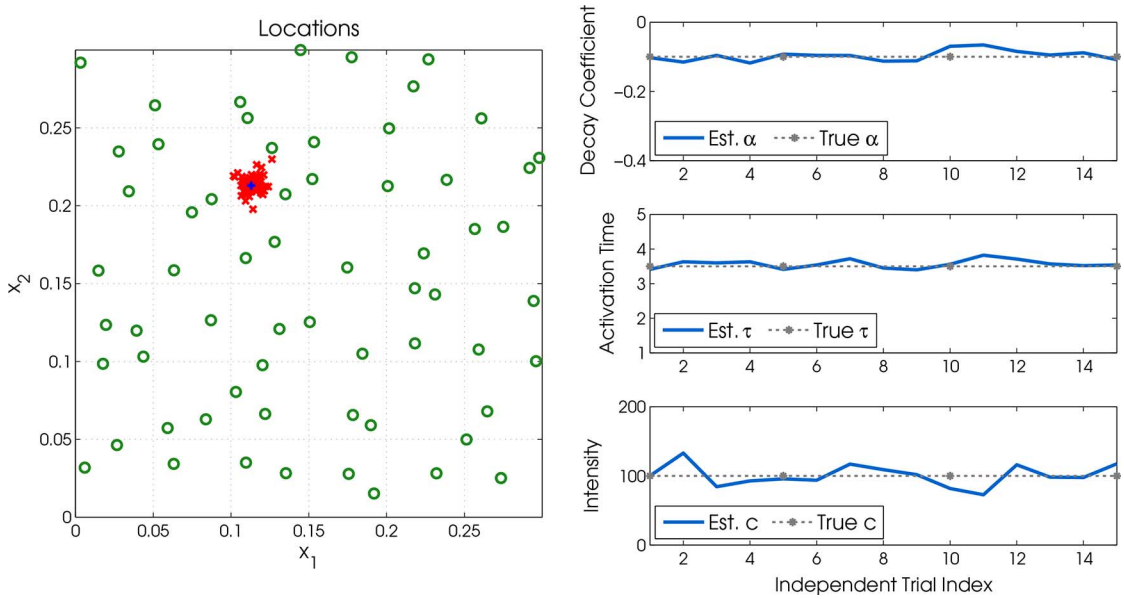

Fig. 4. Estimation of $M = 1$ time-varying diffusion source using 63 randomly distributed sensors. The spatiotemporal samples have SNR equal to 20 dB and the results of 15 independent trials are shown. Intensity $c = 100$; decay coefficient $\alpha = -0.1$; location $\boldsymbol{\xi} = (0.1130, 0.2130)$; and activation time $t = 3.5$ s. Field is sampled for $T_{\text{end}} = 14$ s at a frequency $\frac{1}{\Delta t} = 2$ Hz, $K = 50$ i.e., $k = 0, 1, \ldots, 50$ for the test function family $\Psi_k(\mathbf{x}) = e^{-k(x_1 + \mathrm{j}x_2)}$, $T_1 = 6$ s, $\Delta T = 2$ s and $P = Q + 2 = 5$. The scatter-plot shows the true source locations (blue '+'), the estimated locations (red '×') and one realization of the sensor distribution (green '∘').

TABLE II
NORMALIZED MEAN ABSOLUTE ERROR OF SINGLE SOURCE PARAMETER ESTIMATES USING ALGORITHM 2 (500 INDEPENDENT TRIALS). FIELD IS INDUCED BY THE SINGLE TIME-VARYING SOURCE, $\alpha = -0.1, c = 100, \tau = 3.5$ S AND $\boldsymbol{\xi} = (0.1130, 0.2130)$ AND IS SAMPLED AT $f = \frac{1}{0.5} = 2$ HZ WITH 63 ARBITRARILY PLACED SENSORS. $K = 50, T_1 = 6$ S, $T_{\text{end}} = 14$ S, $P = 5, Q = 3$, AND $\Delta T = 2$ S

	SNR (dB)			
	10	20	30	40
α_m	0.9739	0.3263	0.2665	0.1285
τ_m	0.1493	0.0525	0.0329	0.0258
c_m	1.4016	0.3721	0.2819	0.1677

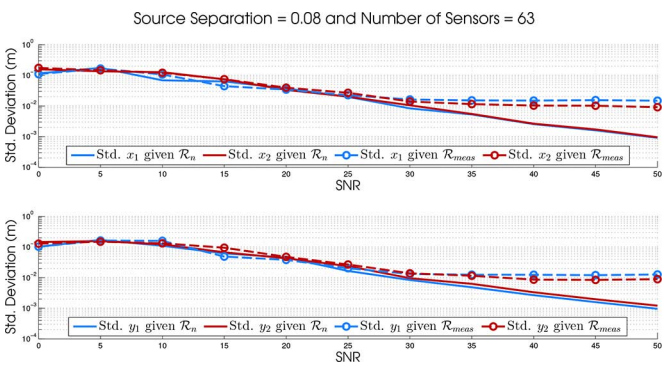

Fig. 5. Standard deviation of location estimates (500 trials) for simultaneous double ($M = 2$) source localization using 63 randomly distributed sensors. $c_1 = c_2 = 1$; $\boldsymbol{\xi}_1 = (0.23, 0.15), \boldsymbol{\xi}_2 = (0.15, 0.15)$; and $t_1 = t_2 = 1.2$ s. $T_{\text{end}} = 10$ s, $\frac{1}{\Delta t} = 1$ Hz and $K = 5$.

B. Estimating Field Sources in Bounded Regions

We simulate the diffusion field in a square region, using the well documented method of *image sources*, by simply introducing virtual sources to model reflections due to the edges of the square. The edges of the bounded region are assumed to be *perfectly insulating*, so that the field incident upon them are all reflected back (i.e., the field does not leak out of the region through its walls). The resulting field therefore diffuses through the square medium as shown in Fig. 6.

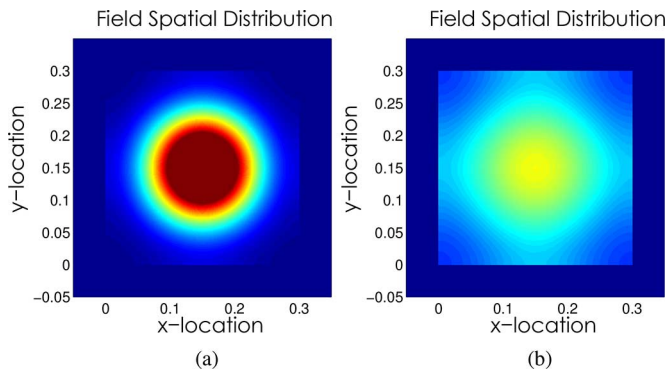

Fig. 6. Spatial field distribution of a single source in a bounded square region at different time instants after source activation. (a) Time $t = 20$ s. (b) Time $t = 50$ s.

1) Source Estimation Results: The results presented in Fig. 7, shows that our algorithm is able to recover multiple sources inducing a field also when the sources are in a bounded region.

C. Experiments With Real Data

In this section, we utilize real temperature data measurements, obtained using a thermal imaging camera, to further validate the proposed source estimation algorithm. Firstly, we outline the experimental setup; specifically we provide a brief overview of how the thermal spatiotemporal samples are obtained and then, we conclude with the results of applying the proposed algorithm to the measured data.

1) Experimental Method: In the real data experiment conducted, a silicon wafer disc of diameter $d = 0.1$ m is used as

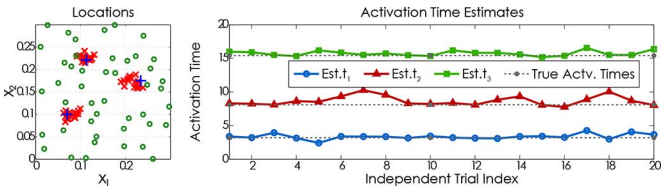

Fig. 7. Estimation of $M = 3$ diffusion sources in a bounded square region, using 45 sensors arbitrarily placed inside the region. The spatiotemporal samples have SNR equal to 20 dB and 20 independent trials are shown. True source parameters: intensities $c_1 = c_2 = c_3 = 1$; locations $\boldsymbol{\xi}_1 = (0.113, 0.221), \boldsymbol{\xi}_2 = (0.234, 0.175), \boldsymbol{\xi}_3 = (0.070, 0.100)$; and activation times $t_1 = 3.2$ s, $t_2 = 8.1$ s, $t_3 = 15.4$ s. Field is sampled for $T_{\text{end}} = 25$ s at a frequency $\frac{1}{\Delta t} = 2$ Hz and $K = 11$ i.e., $k = 0, 1, \ldots, 11$ for the test function family $\Psi_k(\mathbf{x}) = e^{-k(x_1 + \mathrm{j}x_2)}$. The scatter-plot shows the true source locations (blue '+'), the estimated locations (red '×') and the sensor distribution (green '○').

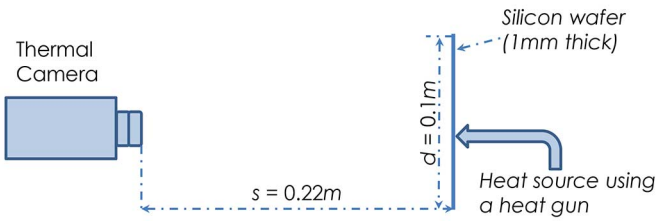

Fig. 8. Experimental Setup.

the diffusion medium. The wafer is placed $s = 0.22$ m from a thermal camera, with the disc lying on the focal plane of the camera; this arrangement, shown in Fig. 8, allows us to measure the entire surface temperature of the silicon plate. We obtain thermal recordings of the disc, at specified frame rates (we use 10 Hz and 25 Hz). A heat gun, with a 1 mm nozzle, is used to apply a localized and instantaneous initial heat source on the opposite face of the silicon plate (i.e., the face opposite that seen by the camera). We continue recording the thermal images for 15 s. We pre-process the recordings by averaging the first few frames and subtracting this average from all frames in the video. This has the effect of imposing the initial temperature distribution of $\approx 0°$C at all spatial locations at time $t = 0$ s.[3]

The camera is properly calibrated so that true xy-locations can be assigned to the 384×288 pixels of each frame. Then spatial sampling, in our setup, corresponds to obtaining samples at a few (specified) pixel locations. These spatial locations are chosen randomly, and one such example is shown as the black circles in 10(a). Moreover, the true value of the source location is the center of the region where the heat source is first observed. For the true activation time, since the frame rate is known, we assume that the source is activated at the frame where we first observe a hot region minus half the sampling interval.

2) Results: The results of our experimentation with real thermal data are summarized in what follows. Fig. 10(a) shows the complete temperature distribution of the monitored region immediately after source activation with the hot (light) region of the map indicating the true source location. Moreover, the estimated source location is shown as the '×'; this estimate has been obtained by applying our proposed algorithm on spatiotemporal measurements obtained at the 13 locations marked by black circles '○'. The temporal evolution of two such sensors are shown in Fig. 9. Note that the sampling frequency $f = \frac{1}{0.52}$ Hz, of the sensors is much lower than the frame rate of the camera. This is achieved by downsampling the actual time measurements.

[3]Note that, due to external factors, we obtain noisy non-zero measurements as seen in Figs. 9 and 10(a).

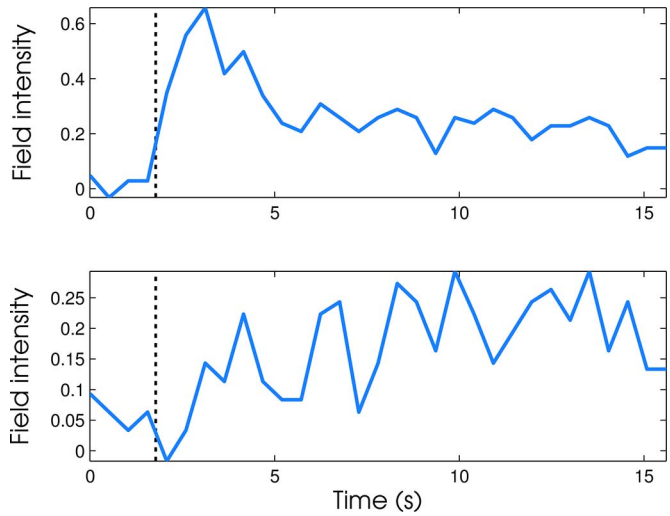

Fig. 9. Measurements of two monitoring sensors obtained at different spatial locations. The dotted vertical line in each plot indicates the instant of source activation.

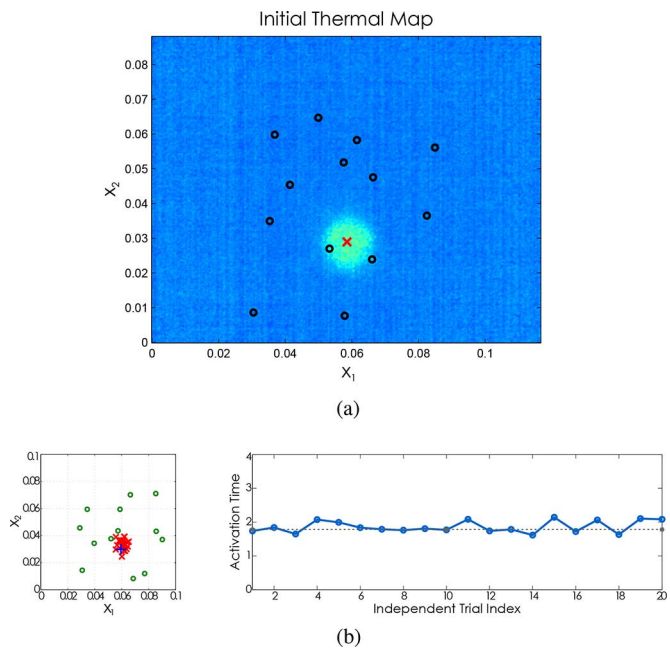

Fig. 10. Estimation of a single instantaneous heat source using real thermal spatiotemporal measurements. The thermal camera is used to capture a sequence of thermal images at 25 Hz for a duration of 16 s. The spatiotemporal samples are obtained by choosing 13 spatial locations (the circles '○' in plots (a) and (b)) at random, and then downsampling in time by a factor of 13; hence $f = \frac{1}{0.52} \approx 1.9231$ Hz and the localization time window $T_{\text{end}} = 12$ s. The true source location is $\boldsymbol{\xi} = (0.0594, 0.0298)$ m and activation time $\tau = 1.7800$ s. In addition, $K = 11$ for the test function family. (a) Shows the thermal image immediately after source activation, the locations of the 13 sensors are indicated by the black circles '○' and the estimated source location by the red '×'. (b) Summarizes the results of 20 independent repetitions of the source estimation algorithm on measurements obtained by a different set of 13 randomly chosen sensor locations; on the left is shown a scatter plot of the estimated source locations (red '×') and the right is plot of the estimated activation times.

TABLE III
MAE OF SINGLE SOURCE PARAMETER ESTIMATES ON REAL THERMAL DATA. THE STATISTICS SHOWN HERE ARE COMPUTED FROM ESTIMATES OF 1000 INDEPENDENT TRIALS, WHERE EACH TRIAL CORRESPONDS TO THE USE OF A DIFFERENT SET OF 13 RANDOMLY DISTRIBUTED SENSORS. THE FIELD IS INDUCED BY THE SINGLE INSTANTANEOUS SOURCE WITH $\tau = 1.7800$ S AND $\boldsymbol{\xi} = (0.0594, 0.0298)$ M AND THE SPATIOTEMPORAL SAMPLES HAVE A SAMPLING FREQUENCY $f = \frac{1}{0.52} \approx 1.9231$ HZ, DURATION OF WINDOW USED IN ESTIMATION $T_{\text{end}} = 12$ S AND $K = 11$ FOR THE TEST FUNCTION FAMILY

	Source Parameter		
	ξ_1	ξ_2	τ
MAE	0.0036	0.0050	0.1544

TABLE IV
SOURCE ESTIMATION RESULTS FOR SIX INDEPENDENT EXPERIMENTAL SET UPS. THE TRUE SOURCE PARAMETERS AND THE ESTIMATES OBTAINED BY OUR SEQUENTIAL ALGORITHM ARE SHOWN. IN PARTICULAR, WE PERFORM SIX INDEPENDENT RECORDINGS (EXPERIMENTS I AND II AT 25 HZ, WHILST EXPERIMENTS III-VI ARE RECORDED AT 10 HZ), THEN THE MEASUREMENTS ARE DOWNSAMPLED SO THAT $f = \frac{1}{0.52}$ AND $f = \frac{1}{0.5}$ FOR EXPERIMENTS I-II AND III-VI RESPECTIVELY. 13 RANDOM LOCATIONS ARE SELECTED AS THE SENSOR LOCATIONS AND ONLY THESE MEASUREMENTS ARE USED BY THE ALGORITHM, OVER $T_{\text{end}} = 12$ S WITH $K = 11$

		TRUE VALUE	ESTIMATE	ABS. ERROR
Experiment I	ξ_1	0.0697	0.0664	0.0033
	ξ_2	0.0310	0.0361	0.0051
	τ	8.7800	8.7883	0.0083
Experiment II	ξ_1	0.0594	0.0590	0.0004
	ξ_2	0.0298	0.0347	0.0049
	τ	1.7800	1.8933	0.1133
Experiment III	ξ_1	0.0600	0.0589	0.0011
	ξ_2	0.0377	0.0451	0.0074
	τ	5.3500	5.5767	0.2267
Experiment IV	ξ_1	0.0606	0.0596	0.0010
	ξ_2	0.0347	0.0323	0.0024
	τ	6.2500	6.4667	0.2167
Experiment V	ξ_1	0.0582	0.0671	0.0089
	ξ_2	0.0359	0.0371	0.0012
	τ	5.3500	5.8917	0.5417
Experiment VI	ξ_1	0.0585	0.0629	0.0044
	ξ_2	0.0365	0.0359	0.0006
	τ	4.9500	5.1833	0.2333

To demonstrate the robustness of the algorithm to the choice of sensor locations, we draw randomly a new set of 13 locations and apply Algorithm 2 on the new spatiotemporal samples. This experiment is repeated 20 times and a scatterplot of the estimated source location and the activation time estimates is shown in Fig. 10(b). The obtained estimates vary marginally about the true values. For statistical significance, we repeat this experiment 1000 times and present the MAE of the location and activation time estimates in Table III. For the location estimates the MAEs are small compared to the dimensions of the monitored region, and also smaller than the average inter-sensor separation. Similarly, the normalized MAE of the activation time is around 0.0867, which is almost an order of magnitude smaller than the temporal sampling interval (0.52 s). Hence on average we observe an absolute error of around 8.67% on the activation time estimates.

We now consider recordings for different source setups. Spatiotemporal measurements are taken for different source activation times and locations; then we attempt to recover the source parameters for each data set using our method. The estimates are presented, alongside the true values, in Table IV, we observe that for each new experiment the parameter estimates remain close to the true values.

VI. CONCLUSION

In this paper, we have presented novel expressions for simultaneously recovering the source parameters of a multi-source diffusion field. Specifically we have considered two types of spatially localized sources: temporally instantaneous and non-instantaneous sources and derived exact inversion formulas for recovering the unknown source parameters given full-field measurements. Then, we properly adapted these formulas to operate in the discrete setup where only sparse spatiotemporal samples of the field are available; and as a result derived and presented novel noise robust methods for estimating multiple field sources.

Simulations carried out on synthetic data have shown that the proposed methods are robust even in the presence of noise and other model mismatches. Furthermore, we have also validated our algorithms using real temperature measurements, obtained experimentally, where the algorithm successfully recovered the location and activation time of the source of a temperature field.

APPENDIX A
PRONY'S METHOD

The systems (11) and (13), as well as (10) for a fixed k or fixed r, are of the general form:

$$\mathcal{R}(k) = \sum_{m=1}^{M} c_m v_m^k, \tag{36}$$

where $c_m, v_m \in \mathbb{C}$ are unknowns. Such a system although linear in the unknown parameters c_m, is nonlinear in the parameters v_m. Hence there is some difficulty associated with finding these nonlinear parameters. Fortunately this problem is well studied and will be solved here by applying Prony's method. A brief overview of the method is given here, for a more in depth treatment see [37].

The method is based on the observation that when the input of a filter having zeros at v_m is the sequence $\mathcal{R}(k)$, then the output will be zero. This filter is called the *annihilating filter*, and has transfer function:

$$A(z) = \sum_{l=0}^{M} a(l) z^{-l} = \prod_{m=1}^{M} (1 - v_m z^{-1}), \tag{37}$$

where $a(k)$ is the impulse response of the filter $A(z)$. Specifically,

$$\begin{aligned}(a * \mathcal{R})(k) &= \sum_{l=0}^{M} a(l) \mathcal{R}(k-l) \\ &= \sum_{l=0}^{M} a(l) \sum_{m=1}^{M} c_m v_m^{k-l} \\ &= \underbrace{\sum_{l=0}^{M} a(l) v_m^{-l}}_{=A(v_m)} \sum_{m=1}^{M} c_m v_m^k = 0,\end{aligned} \tag{38}$$

since $A(z)|_{z=v_m} = 0$. Given the sequence $\mathcal{R}(k)$, the convolution between $(a * \mathcal{R})(k)$ may be written in the matrix/vector form as $\mathbf{Ra} = \mathbf{0}$, such that:

$$\begin{pmatrix} \vdots & \vdots & \cdots & \vdots \\ \mathcal{R}(M) & \mathcal{R}(M-1) & \cdots & \mathcal{R}(0) \\ \mathcal{R}(M+1) & \mathcal{R}(M) & \cdots & \mathcal{R}(1) \\ \vdots & \vdots & \ddots & \vdots \\ \mathcal{R}(2M) & \mathcal{R}(2M-1) & \cdots & \mathcal{R}(M) \\ \vdots & \vdots & \cdots & \vdots \end{pmatrix} \begin{pmatrix} a(0) \\ a(1) \\ \vdots \\ a(M) \end{pmatrix} = \mathbf{0}. \quad (39)$$

The matrix $\mathbf{R}$ is rank deficient with rank M and is therefore overdetermined. Imposing $a(0) = 1$ enforces a unique solution—since there are now M coefficients of the filter to be found—therefore we need at least $2M$ consecutive terms of the sequence $\{\mathcal{R}(k)\}_{k=0}^{K}$; i.e., $K \geq 2M - 1$. Once $\mathbf{a}$ has been found, then the values of v_m are simply the roots of the polynomial $A(z)$. Finally the amplitudes c_m can be determined by simply taking any M equations in (36) and solving the resultant Vandermonde system.

In the presence of model mismatch, (39) is no longer satisfied exactly, yet minimizing the Euclidean norm $\|\mathbf{Ra}\|^2$ subject to $\|\mathbf{a}\|^2 = 1$, gives a good estimate for $\mathbf{a}$ [40]. Hence, the Total Least-Squares (TLS) method is used to solve for $\mathbf{a}$, where $\mathbf{a}$ is chosen to be the eigenvector which corresponds to the smallest eigenvalue of the matrix $\mathbf{R}^\top\mathbf{R}$. More details of the TLS method can be found in [40].

ACKNOWLEDGMENT

The authors would like to thank Dr. David Looney, Dr. Valentin Goverdovsky and Mr. Tasmiat Rahman at Imperial College, London, for providing us with the equipments used in conducting the real temperature data experiments.

REFERENCES

[1] J. Murray-Bruce and P. L. Dragotti, "Spatio-temporal sampling and reconstruction of diffusion fields induced by point sources," presented at the 39th IEEE Int. Conf. Acous., Speech, Signal Process. (ICASSP), Florence, Italy, May 2014.

[2] J. Murray-Bruce and P. L. Dragotti, "Reconstructing diffusion fields sampled with a network of arbitrarily distributed sensors," presented at the Eur. Signal Process. Conf. (EUSIPCO), Lisbon, Portugal, Sep. 2014.

[3] B. A. Egan and J. R. Mahoney, "Numerical modeling of advection and diffusion of urban area source pollutants," *J. Appl. Meteorol.*, vol. 11, no. 2, pp. 312–322, 1972.

[4] K. Langendoen, A. Baggio, and O. Visser, "Murphy loves potatoes: Experiences from a pilot sensor network deployment in precision agriculture," in *Proc. 20th Int. Parallel Distrib. Process. Symp. (IPDPS)*, Apr. 2006, p. 8.

[5] J. Matthes, L. Gröll, and H. B. Keller, "Source localization by spatially distributed electronic noses for advection and diffusion," *IEEE Trans. Signal Process.*, vol. 53, no. 5, pp. 1711–1719, May 2005.

[6] M. Chino, H. Nakayama, H. Nagai, H. Terada, G. Katata, and H. Yamazawa, "Preliminary estimation of release amounts of 131i and 137cs accidentally discharged from the fukushima daiichi nuclear power plant into the atmosphere," *J. Nucl. Sci. Technol.*, vol. 48, no. 7, pp. 1129–1134, 2011.

[7] C. Shackelford and D. Daniel, "Diffusion in saturated soil I: Background," *J. Geotechn. Eng.*, vol. 117, no. 3, pp. 467–484, 1991.

[8] D. Brooks, R. P. Dick, R. Joseph, and L. Shang, "Power, thermal, and reliability modeling in nanometer-scale microprocessors," *IEEE Micro*, vol. 27, no. 3, pp. 49–62, May 2007.

[9] J. Ranieri, A. Vincenzi, A. Chebira, D. A. Alonso, and M. Vetterli, "EigenMaps: Algorithms for optimal thermal maps extraction and sensor placement on multicore processors," in *Proc. 49th Design Autom. Conf. (DAC)*, San Francisco, 2012, pp. 636–641, ser. Design Automation Conference (DAC'12), ACM.

[10] R. Bianchini and R. Rajamony, "Power and energy management for server systems," *IEEE Comput.*, vol. 37, no. 11, pp. 68–76, Nov. 2004.

[11] I. Dokmanic, J. Ranieri, A. Chebira, and M. Vetterli, "Sensor networks for diffusion fields: Detection of sources in space and time," in *Proc. 49th Allerton Conf. Commun., Control, Comput. (Allerton)*, Monticello, IL, USA, Sep. 2011, pp. 1552–1558.

[12] J. Ranieri, I. Dokmanic, A. Chebira, and M. Vetterli, "Sampling and reconstruction of time-varying atmospheric emissions," presented at the 37th IEEE Int. Conf. Acoust., Speech, Signal Process. (ICASSP), New York, NY, USA, Mar. 2012, IEEE.

[13] J. Ranieri, Y. Lu, A. Chebira, and M. Vetterli, "Sampling and reconstructing diffusion fields with localized sources," in *Proc. IEEE Int. Conf. Acoust., Speech, Signal Process. (ICASSP)*, May 2011, pp. 4016–4019.

[14] Y. M. Lu, P. L. Dragotti, and M. Vetterli, "Localizing point sources in diffusion fields from spatiotemporal samples," presented at the 9th Int. Conf. Sampl. Theory Appl. (SampTa), Singapore, 2011.

[15] Y. M. Lu, P. L. Dragotti, and M. Vetterli, "Localization of diffusive sources using spatiotemporal measurements," in *Proc. 49th IEEE Annu. Allerton Conf. Commun., Control, Comput. (Allerton)*, Monticello, IL, USA, Sep. 2011, pp. 1072–1076.

[16] C. Le Niliot and F. Lefevre, "Multiple transient point heat sources identification in heat diffusion: Application to numerical two-and three-dimensional problems," *Numer. Heat Transfer: Part B: Fundam.*, vol. 39, no. 3, pp. 277–301, 2001.

[17] M. Rostami, N.-M. Cheung, and T. Quek, "Compressed sensing of diffusion fields under heat equation constraint," in *Proc. IEEE Int. Conf. Acoust., Speech, Signal Process. (ICASSP)*, Vancouver, Canada, May 2013, pp. 4271–4274.

[18] G. Reise, G. Matz, and K. Grochenig, "Distributed field reconstruction in wireless sensor networks based on hybrid shift-invariant spaces," *IEEE Trans. Signal Process.*, vol. 60, no. 10, pp. 5426–5439, 2012.

[19] T. van Waterschoot and G. Leus, "Static field estimation using a wireless sensor network based on the finite element method," in *Proc. 4th IEEE Int. Workshop Comput. Adv. Multi-Sensor Adapt. Process. (CAMSAP)*, Dec. 2011, pp. 369–372.

[20] A. Kumar, P. Ishwar, and K. Ramchandran, "On distributed sampling of smooth non-bandlimited fields," in *Proc. 3rd Int. Symp. Inf. Process. Sensor Netw.*, 2004, pp. 89–98.

[21] J. Ranieri and M. Vetterli, "Sampling and reconstructing diffusion fields in presence of aliasing," presented at the IEEE Int. Conf. Acoust., Speech, Signal Process. (ICASSP), Vancouver, Canada, May 2013.

[22] G. Reise and G. Matz, "Distributed sampling and reconstruction of nonbandlimited fields in sensor networks based on shift-invariant spaces," in *Proc. IEEE Int. Conf. Acoust., Speech, Signal Process. (ICASSP)*, Taipei, Taiwan, 2009, pp. 2061–2064.

[23] H. C. Elman, D. J. Silvester, and A. J. Wathen, *Finite Elements and Fast Iterative Solvers: With Applications in Incompressible Fluid Dynamics*. New York, NY, USA: Oxford Univ. Press, 2005.

[24] S. C. Brenner and R. Scott, *The Mathematical Theory of Finite Element Methods*. New York, NY, USA: Springer, 2008, vol. 15.

[25] T. van Waterschoot and G. Leus, "Distributed estimation of static fields in wireless sensor networks using the finite element method," in *Proc. IEEE Int. Conf. Acoust., Speech, Signal Process. (ICASSP)*, Kyoto, Japan, Mar. 2012, pp. 2853–2856.

[26] M. Rostami, N.-M. Cheung, and T. Quek, "Compressed sensing of diffusion fields under heat equation constraint," in *Proc. IEEE Int. Conf. Acoust., Speech, Signal Process. (ICASSP)*, Vancouver, Canada, May 2013, pp. 4271–4274.

[27] A. Nehorai, B. Porat, and E. Paldi, "Detection and localization of vapor-emitting sources," *IEEE Trans. Signal Process.*, vol. 43, no. 1, pp. 243–253, Jan. 1995.

[28] J. Weimer, B. Sinopoli, and B. H. Krogh, "Multiple source detection and localization in advection-diffusion processes using wireless sensor networks," in *Proc. 30th IEEE Real-Time Syst. Symp. (RTSS)*, Washington, DC, USA, 2009, pp. 333–342.

[29] Z. Yong, Z. Hui, G. Dongqiang, and W. Zhihua, "Determination of chemical point source using distributed algorithm in sensors network," in *Proc. 24th Chin. Control Decision Conf. (CCDC)*, May 2012, pp. 3373–3377.

[30] F. Sawo, K. Roberts, and U. D. Hanebeck, "Bayesian estimation of distributed phenomena using discretized representations of partial differential equations," in *Proc. 3rd IEEE Int. Conf. Inf. Control, Autom., Robot. (ICINCO)*, Aug. 2006, pp. 16–23.
[31] C. Le Niliot, F. Rigollet, and D. Petit, "An experimental identification of line heat sources in a diffusive system using the boundary element method," *Int. J. Heat Mass Transfer*, vol. 43, no. 12, pp. 2205–2220, 2000.
[32] Y. M. Lu and M. Vetterli, "Spatial super-resolution of a diffusion field by temporal oversampling in sensor networks," in *Proc. IEEE Int. Conf. Acoust., Speech, Signal Process. (ICASSP)*, 2009, pp. 2249–2252.
[33] Y. M. Lu and M. Vetterli, "Distributed spatio-temporal sampling of diffusion fields from sparse instantaneous sources," in *Proc. 3rd IEEE Int. Workshop Comput. Adv. Multi-Sensor Adapt. Process. (CAMSAP)*, Aruba, Dutch Antilles, 2009, pp. 205–208, IEEE.
[34] N. Antonello, T. van Waterschoot, M. Moonen, and P. A. Naylor, "Source localization and signal reconstruction in a reverberant field using the FDTD method," in *Proc. 22nd Eur. Signal Process. Conf. (EUSIPCO)*, Sept. 2014, pp. 301–305.
[35] G. Reise and G. Matz, "Clustered wireless sensor networks for robust distributed field reconstruction based on hybrid shift-invariant spaces," in *Proc. IEEE 10th Workshop Signal Process. Adv. Wireless Commun. (SPAWC)*, 2009, pp. 66–70.
[36] G. R. de Prony, "Essai expérimental et analytique: sur les lois de la dilatabilité des fluides élastiques et sur celles de la force expansive de la vapeur de l'Alkool, à différentes températures," *J. de l'école Polytechn.*, vol. 1, 1795.
[37] P. Stoica and R. Moses, *Introduction to Spectral Analysis*. Englewood Cliffs, NJ, USA: Prentice-Hall, 1997.
[38] M. Vetterli, P. Marziliano, and T. Blu, "Sampling signals with finite rate of innovation," *IEEE Trans. Signal Process.*, vol. 50, no. 6, pp. 1417–1428, Jun. 2002.
[39] P.-L. Dragotti, M. Vetterli, and T. Blu, "Sampling moments and reconstructing signals of finite rate of innovation: Shannon meets strang-fix," *IEEE Trans. Signal Process.*, vol. 55, no. 5, pp. 1741–1757, 2007.
[40] T. Blu, P.-L. Dragotti, M. Vetterli, P. Marziliano, and L. Coulot, "Sparse sampling of signal innovations," *IEEE Signal Process. Mag.*, vol. 25, no. 2, pp. 31–40, Mar. 2008.
[41] J. Oñativia, S. R. Schultz, and P. L. Dragotti, "A finite rate of innovation algorithm for fast and accurate spike detection from two-photon calcium imaging," *J. Neural Eng.*, vol. 10, no. 4, p. 046017, 2013.
[42] S. Andrieux and A. B. Abda, "Identification of planar cracks by complete overdetermined data: Inversion formulae," *Inverse Problems*, vol. 12, no. 5, p. 553, 1996.
[43] T. Bannour, A. B. Abda, and M. Jaoua, "A semi-explicit algorithm for the reconstruction of 3D planar cracks," *Inverse Problems*, vol. 13, no. 4, p. 899, 1997.
[44] N. Auffray, M. Bonnet, and S. Pagano, "Identification of transient heat sources using the reciprocity gap," *Inverse Problems Sci. Eng.*, vol. 21, no. 4, pp. 721–738, 2013.
[45] D. Kandaswamy, T. Blu, and D. Van De Ville, "Analytic sensing: Noniterative retrieval of point sources from boundary measurements," *SIAM J. Sci. Comput.*, vol. 31, no. 4, pp. 3179–3194, 2009.
[46] G. Dahlquist and Å. Björck, *Numerical Methods in Scientific Computing*, ser. SIAM e-books. Philadelphia, PA, USA: SIAM, 2008, vol. 1, no. v. 1.
[47] K. Georg, "Approximation of integrals for boundary element methods," *SIAM J. Sci. Statist. Comput.*, vol. 12, no. 2, pp. 443–453, 1991.
[48] M. de Berg, O. Cheong, M. van Kreveld, and M. Overmars, *Computational Geometry: Algorithms and Applications*, 3rd ed. Santa Clara, CA, USA: Springer-Verlag, 2008.
[49] J. A. Cadzow, "Signal enhancement—A composite property mapping algorithm," *IEEE Trans. Acoust., Speech, Signal Process.*, vol. 36, no. 1, pp. 49–62, Jan. 1988.

John Murray-Bruce (S'14) is currently a Research Assistant with the Electrical and Electronic Engineering Department at Imperial College London, where he is also studying for the Ph.D. degree in electrical and electronic engineering under the supervision of Professor Pier Luigi Dragotti. In 2012 he graduated from Imperial College London with the Master's degree (first class) and was awarded the Institute of Engineering and Technology (IET) Prize for 'Best All round Performance.' His current research interests are in interpolation, approximation and sampling theory, distributed algorithms, as well as, inverse problems of physical fields.

Pier Luigi Dragotti (M'02–SM'11) is Professor of Signal Processing with the Electrical and Electronic Engineering Department at Imperial College London. He received the Laurea degree (*summa cum laude*) in electrical and electronic engineering from the University of Naples Federico II, Naples, Italy, in 1997; the Master's degree in communications systems from the Swiss Federal Institute of Technology of Lausanne (EPFL), Lausanne, Switzerland, in 1998, and the Ph.D. degree from EPFL in April 2002. He has held several visiting positions at different universities and research centers. He was a Visiting Student with Stanford University, Stanford, CA, USA, in 1996, a Researcher with the Mathematics of Communications Department, Bell Labs, Lucent Technologies, Murray Hill, NJ, USA, in 2000 and a Visiting Scientist with the Massachusetts Institute of Technology, Cambridge, MA, USA, in 2011. He was Technical Co-Chair for the European Signal Processing Conference in 2012, an Associate Editor of the IEEE TRANSACTIONS ON IMAGE PROCESSING from 2006 to 2009 and an Elected Member of the IEEE Image, Video and Multidimensional Signal Processing Technical Committee (2008–2013). Currently he is an elected member of the IEEE Signal Processing Theory and Method Technical Committee. He is a recipient of the ERC Starting Investigator Award for the project RecoSamp. His work includes sampling theory, wavelet theory and its applications, image and video compression, image-based rendering, and image super-resolution.